8-2016

WRF Forecasts of Great Plains Nocturnal Low-Level Jet-Driven MCSs. Part I: Correlation between Low-Level Jet Forecast Accuracy and MCS Precipitation Forecast Skill

Brian J. Squitieri
Iowa State University, brianjs@iastate.edu

William A. Gallus Jr.
Iowa State University, wgallus@iastate.edu

WRF Forecasts of Great Plains Nocturnal Low-Level Jet-Driven MCSs. Part I: Correlation between Low-Level Jet Forecast Accuracy and MCS Precipitation Forecast Skill

Abstract
The Great Plains low-level jet (LLJ) fosters an environment that supports nocturnal mesoscale convective systems (MCSs) across the central United States during the summer months. The current study examines if LLJ forecast accuracy correlates with MCS precipitation forecast skill in 4-km WRF runs. LLJs were classified based on their synoptic background as either strongly forced, cyclonic flow (type C) or weakly forced, anticyclonic flow inertial oscillation driven (type A). Large-scale variables associated with the LLJ were examined. For all LLJs inclusive and the subset of type C LLJs alone, the forecast accuracy of the LLJ total wind direction significantly correlated with MCS precipitation forecast skill. For type C LLJ cases, where predictive skill for MCSs was higher overall, the LLJ ageostrophic wind direction forecast accuracy significantly correlated with MCS precipitation forecast skill during the LLJ and MCS developmental stages, with potential temperature and moisture forecast accuracy correlating well with the forecast skill of mature MCSs. Statistically significant correlations were mainly absent between MCS precipitation forecast skill and LLJ forecast accuracy for type A cases. It is thus suggested that either non-LLJ factors like most unstable convective available potential energy (MUCAPE) or most unstable convective inhibition (MUCIN) fields within close proximity of MCSs, or factors on smaller scales than analyzed (such as gravity waves or bores), may have the greatest potential influence on MCS precipitation forecast skill in LLJ-induced MCS cases in an ambient weakly forced synoptic regime.

Keywords
Circulation/ Dynamics, Convective storms/systems, Atm/Ocean Structure/ Phenomena, Jets, Forecasting, Forecast verification/skill, Mesoscale forecasting, Models and modeling, Mesoscale models, Model errors

Disciplines
Atmospheric Sciences | Climate | Meteorology

Comments
This article is published as Squitieri, Brian J., and William A. Gallus Jr. "WRF forecasts of Great Plains nocturnal low-level jet-driven MCSs. Part I: Correlation between low-level jet forecast accuracy and MCS precipitation forecast skill." Weather and Forecasting 31, no. 4 (2016): 1301-1323. DOI: 10.1175/WAF-D-15-0151.1. Posted with permission.

WRF Forecasts of Great Plains Nocturnal Low-Level Jet-Driven MCSs. Part I: Correlation between Low-Level Jet Forecast Accuracy and MCS Precipitation Forecast Skill

BRIAN J. SQUITIERI AND WILLIAM A. GALLUS JR.

Department of Geological and Atmospheric Sciences, Iowa State University, Ames, Iowa

(Manuscript received 3 November 2015, in final form 23 May 2016)

ABSTRACT

The Great Plains low-level jet (LLJ) fosters an environment that supports nocturnal mesoscale convective systems (MCSs) across the central United States during the summer months. The current study examines if LLJ forecast accuracy correlates with MCS precipitation forecast skill in 4-km WRF runs. LLJs were classified based on their synoptic background as either strongly forced, cyclonic flow (type C) or weakly forced, anticyclonic flow inertial oscillation driven (type A). Large-scale variables associated with the LLJ were examined. For all LLJs inclusive and the subset of type C LLJs alone, the forecast accuracy of the LLJ total wind direction significantly correlated with MCS precipitation forecast skill. For type C LLJ cases, where predictive skill for MCSs was higher overall, the LLJ ageostrophic wind direction forecast accuracy significantly correlated with MCS precipitation forecast skill during the LLJ and MCS developmental stages, with potential temperature and moisture forecast accuracy correlating well with the forecast skill of mature MCSs. Statistically significant correlations were mainly absent between MCS precipitation forecast skill and LLJ forecast accuracy for type A cases. It is thus suggested that either non-LLJ factors like most unstable convective available potential energy (MUCAPE) or most unstable convective inhibition (MUCIN) fields within close proximity of MCSs, or factors on smaller scales than analyzed (such as gravity waves or bores), may have the greatest potential influence on MCS precipitation forecast skill in LLJ-induced MCS cases in an ambient weakly forced synoptic regime.

1. Introduction

Mesoscale convective systems (MCSs) are the primary source of precipitation across the Great Plains and Midwest during the summer months (Fritsch et al. 1986; Stensrud 1996; Ashley et al. 2003; Jirak and Cotton 2007; Coniglio et al. 2010) and provide the rainfall needed for agricultural purposes; thus, better forecasts of nocturnal convection benefit farmers (Jirak et al. 2003). Nocturnal MCS development and sustenance is often tied to the occurrence of the Great Plains southerly low-level jet (LLJ) (Cotton et al. 1989; Augustine and Caracena 1994; Mitchell et al. 1995; Higgins et al. 1997; French and Parker 2010), a narrow current of air with a wind speed maximum located between 300 and 1000 m above ground level (AGL) (Bonner and Paegle 1970; Mitchell et al. 1995; Whiteman et al. 1997; Song et al. 2005). Uccellini (1980) classified LLJs based on their synoptic environments, finding that LLJs were typically produced by lee cyclogenesis east of the Rocky Mountains and by the inertial oscillation and terrain sloping/heating processes described in Blackadar (1957) and Bonner and Paegle (1970). In Markowski and Richardson (2010), dynamically driven pressure-gradient- and inertial-oscillation-induced LLJs are referred to as the low-level jet stream and low-level wind maximum, respectively. Given the differences between these LLJ types and the supporting synoptic background, Stensrud (1996) claimed it is vital to distinguish between LLJ types for any comprehensive research. For the present work, it was hypothesized that better simulations of the LLJ, regardless of synoptic background, may yield better forecasts of MCS precipitation (Mitchell et al. 1995; French and Parker 2010).

Hu et al. (2010) (using surface and aircraft data for observations) and Coniglio et al. (2013) (using soundings from National Weather Service operations and the Midcontinent Convective Clouds Experiment as

Corresponding author address: Brian Squitieri, Iowa State University, 3018 Agronomy Hall, Ames, IA 50011.
E-mail: brianjs@iastate.edu

DOI: 10.1175/WAF-D-15-0151.1

observations) and Schumacher et al. (2013) (using NARR, radiosonde, and wind profiler observations) ran the WRF under multiple local and nonlocal mixing-based planetary boundary layer (PBL) schemes and found that the Mellor–Yamada–Janjić (MYJ) scheme resulted in a boundary layer that was too cool and moist. As such, Hu et al. (2010) found that the MYJ simulated a low-level wind maximum (likely the entrance region of an LLJ) as being too strong, while the Yonsei University (YSU) scheme was too weak with regard to wind magnitude, also noted by Schumacher et al. (2013). The MYJ scheme did not factor in entrainment from the top of the PBL, and thus its boundary layer depth became too shallow, too quickly, likely promoting the strong wind speeds rapidly developing above the PBL. It should be noted that this study was conducted in south Texas during the summer months; hence, the core of the LLJ was likely not sampled and conclusions on PBL schemes with respect to LLJ development could not be made. Coniglio et al. (2013) found that the Mellor–Yamada–Nakanishi–Niino (MYNN 2.5) scheme alleviated many of the temperature and moisture biases within the PBL, lending higher confidence for its use in simulating pre-convective environments.

Within the last decade, methods for evaluating forecast precipitation have changed with the implementation of finer horizontal grid spacing. Ebert (2008) noted that using traditional gridpoint metrics for model verification tended to punish reasonable forecasts given the model's incapability to simulate a precipitation scenario with near perfection. To lend fair credibility to more accurate model forecasts, Ebert devised a "fuzzy" logic approach that calculated precipitation skill scores by counting correct forecast grid points within larger grid squares of influence in place of relying on exact gridpoint matches. This neighborhood approach led to the development of the fractions skill score (FSS) that rewarded forecasts with smaller timing and or spatial displacements compared to those with larger errors. These findings were further supported by Roberts and Lean (2008), particularly for model forecasts at 1.5-km horizontal grid spacing, where convective features seemed to be better resolved. Finally, Clark et al. (2010) derived a neighborhood approach for the equitable threat score (ETS) and associated frequency bias, where correct forecast hits were counted within a radius of influence for a given grid point. Similar to Ebert (2008) and Roberts and Lean (2008), the leniency granted to counting hits in the neighborhood ETS calculation greatly improved forecast skill scores for cases where small displacements in precipitation forecasts existed, particularly for heavy rainfall events in convection-allowing models.

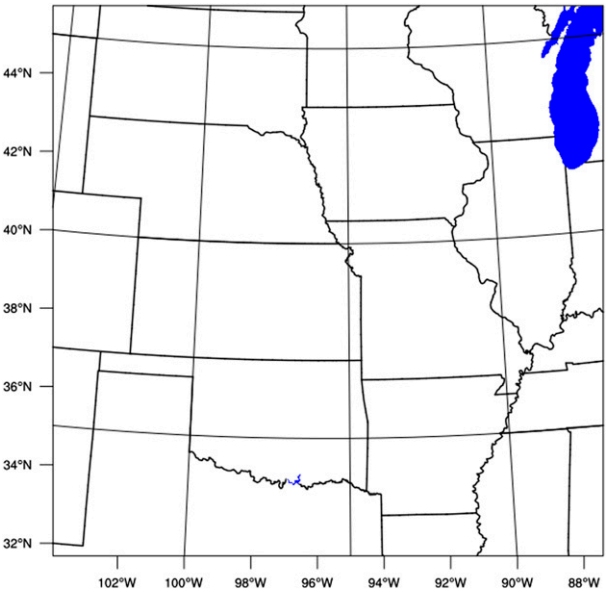

FIG. 1. Domain shared by the 4-km WRF and 0-h 13-km RUC analyses.

While the previous works cited aimed at improving the accuracy of the boundary layer and LLJs along with MCS forecast skill, little work has been done focusing on the relationship between the accuracy of simulated LLJs and the subsequent forecast MCS quantitative precipitation forecast (QPF) skill in real cases using high spatial resolution. The present research aims to simulate real cases of LLJ and subsequent MCS evolution with high vertical and horizontal resolution using the 4-km WRF with multiple PBL and microphysics (MP) schemes. It should be noted that LLJs are not the only important factors influencing development and sustenance of MCSs, though reviewing these additional features is beyond the scope of this paper. This research focuses on the hypothesis that cases with better simulations of the LLJ would yield better MCS precipitation forecasts. Correlations of forecast accuracy of large-scale LLJ variables and forecast skill for MCS precipitation will be emphasized both for all cases inclusive, and for type C and A LLJ cases separately.

2. Data and methodology

With in situ observations of winds in the lower troposphere lacking for validation of high spatial resolution modeling, 13-km RUC analyses (NCDC 2015b) were substituted for in situ data as in Thompson et al. (2003), Hane et al. (2008), Schumacher and Johnson (2009), Coniglio et al. (2010), and Snively and Gallus (2014). RUC output originally on constant pressure levels was interpolated to levels of constant height

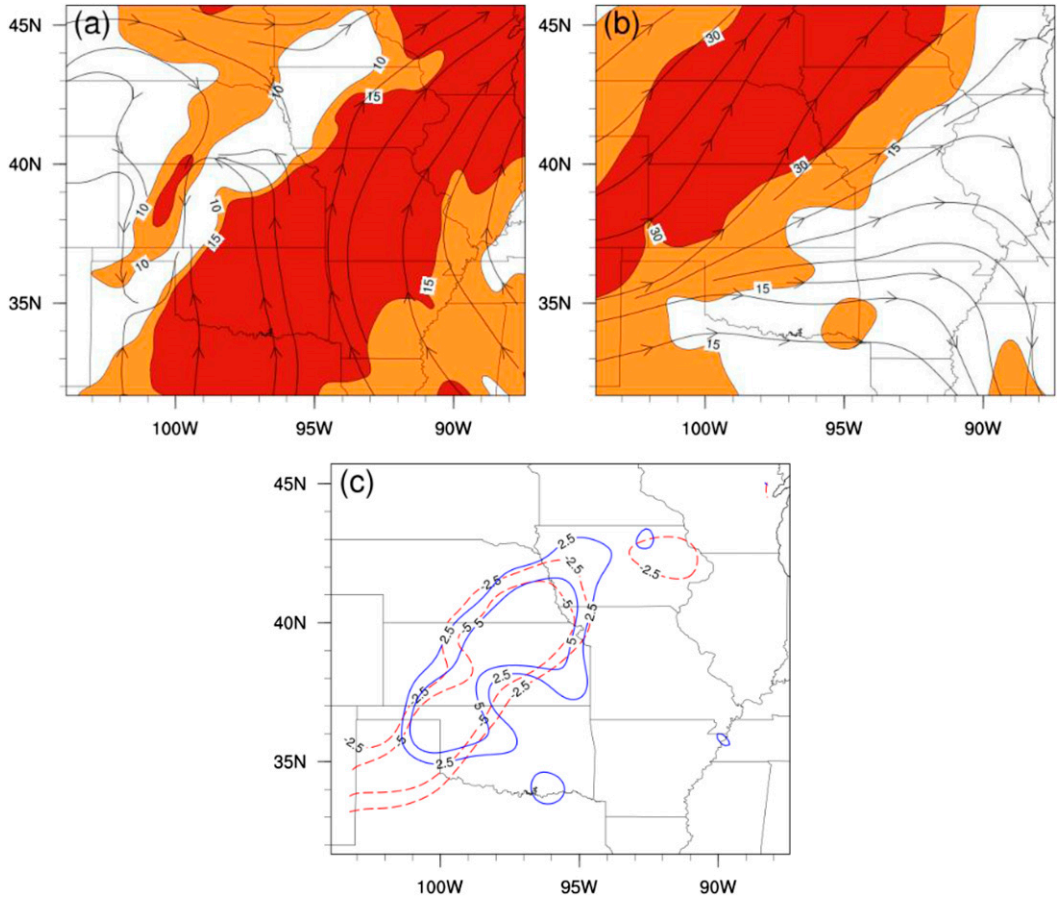

FIG. 2. For the type C case at 0600 UTC 24 May 2007 in the 0-h 13-km RUC analysis, (a) 900-mb streamlines and wind magnitudes color filled at 10 and 15 m s^{-1}, (b) 200-mb streamlines and wind magnitudes color filled at 15 and 30 m s^{-1}, and (c) 900-mb convergence (10^{-5} s^{-1}) in red and 200-mb divergence in blue (10^{-5} s^{-1}).

AGL. Given the few observational datasets available for evaluating LLJ structure, it is difficult to tell how well the RUC analyses represent the LLJ. Although some biases may be present in the RUC analyses, past studies found any problems to be relatively minor and the analyses to be an adequate representation of the observed conditions.

The present research employed version 3.5 of the ARW (Skamarock et al. 2008) model with 4-km horizontal grid spacing. Vertical grid spacing on terrain-following hydrostatic pressure coordinates consisted of 50 manually defined eta levels, with 28 levels below 850 hPa, allowing for very fine vertical resolution of the LLJ. The selected domain spanned a 1600 km × 1600 km area across the eastern Great Plains and Midwest states (Fig. 1). All runs were initialized at 1200 UTC prior to the case studied in order to capture the diurnal effects on the boundary layer and resultant impacts on later LLJ evolution. Thirty-one cases were chosen based on an LLJ being present in the RUC analyses, along with subsequent MCS development (determined via archived mosaic radar data) as well as the availability of 12-km NAM forecast output (NCDC 2015a) used to initialize the WRF lateral and boundary conditions, 13-km RUC analyses, and stage IV data (applicable for 2007 onward, hence all cases included within the 2007–14 period). LLJs were classified based on Bonner's (1968) criteria with the LLJ maximum reaching the Bonner II criteria and the core establishing a minimum of Bonner I criteria as the threshold for a case being selected for study. LLJs were also classified based on their synoptic environment, similar to Uccellini (1980). A streamline analysis with wind magnitudes at 900 and 200 hPa along with overlaid 900- and 200-hPa divergence was employed to determine LLJ type. The evaluation of the coupling of 900-hPa convergence and 200-hPa divergence to determine LLJ type stems from the work of Uccellini and Johnson (1979), who stated that LLJs and upper-level jet streaks are coupled in strongly forced synoptic setups, where the convergent exit region of an LLJ is overrun by a divergent entrance region of an upper-level jet streak, allowing for

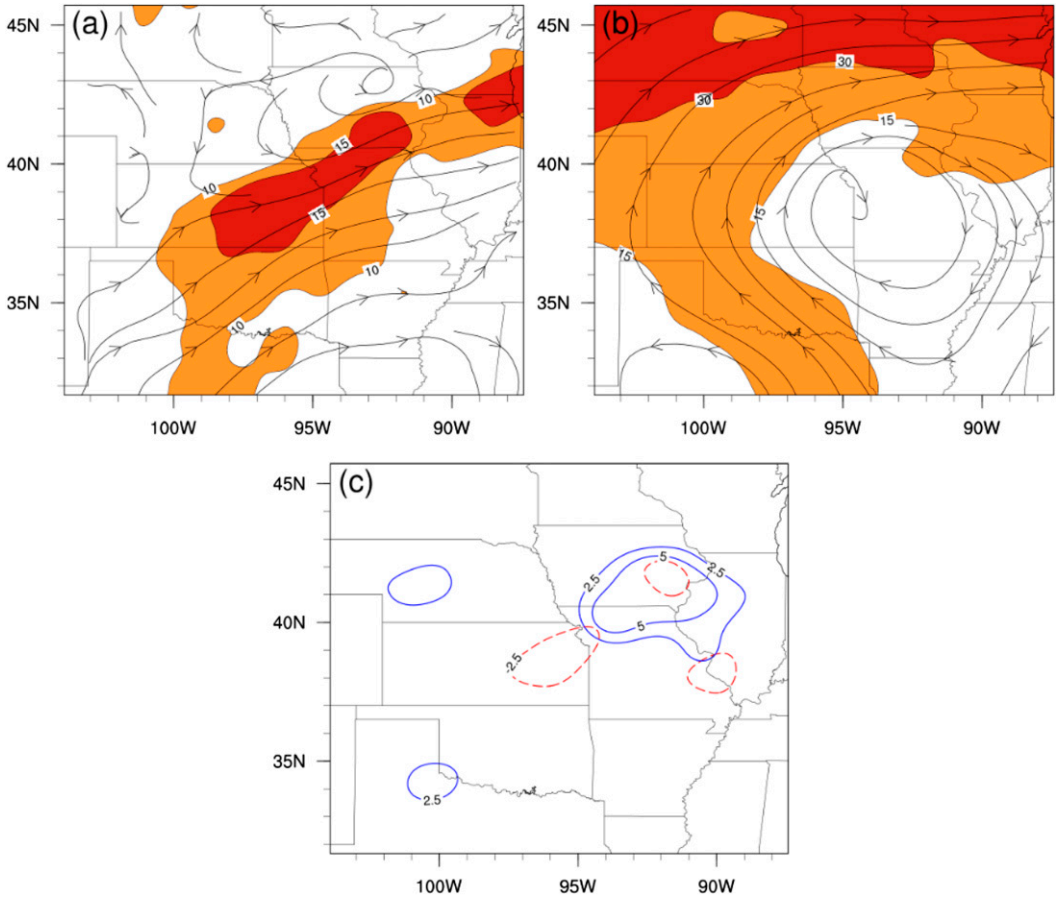

FIG. 3. As in Fig. 2, but for the type A case at 0600 UTC 9 Aug 2010.

large-scale vertical motion (which often promotes widespread storm organization and severe weather). Cases where strong 900-hPa southerly flow (where magnitudes reached or surpassed 15 m s^{-1}) and strong cyclonic flow at 200 hPa (where magnitudes reached or surpassed 30 m s^{-1}) are present and where 900-hPa convergence is coupled with 200-hPa divergence are considered cyclonic LLJ events, representative of the pressure-gradient-induced low-level jet streams alluded to in Markowski and Richardson (2010). An illustration of this method for manual classification is shown in Fig. 2 (referred to henceforth as type C LLJs). Low-level wind maxima (Markowski and Richardson 2010), where strong southerly flow is still present at 900 hPa but with weak anticyclonic flow at 200 hPa and little to no jet coupling, are considered anticyclonic LLJs or type A (an example is shown in Fig. 3), where the inertial oscillation (Blackadar 1957), terrain sloping, and heating (Wexler 1961; Bonner and Paegle 1970; Uccellini 1980; Pan et al. 2004; Parish and Oolman 2010) play the biggest roles in forcing the LLJ. Of the 31 total cases, 16 were of type C and 15 were of type A LLJ regimes.

In addition to the LLJ criterion for case selection, associated MCSs needed to exhibit a linear or occluding structure, as defined in Blanchard (1990). MCSs that exhibited Blanchard's definition of chaotic structure were accepted so long as intense convective elements within the chaotic structure were observed for at least 3 h during evolution. MCSs that were located closer to the center of the WRF domain were selected to minimize negative feedback from lateral boundaries.

Limited sensitivity tests were also performed to understand the role of the MP and PBL schemes in the correlation of LLJ and MCS precipitation errors. To determine if hydrometeor distribution would affect the correlation of forecast skill, WRF runs for each case were conducted under two different MP schemes. The WRF single-moment 6-class (WSM6) scheme was chosen because it was specially developed for high-resolution simulations involving ice, graupel, and snow processes in atmospheric cloud simulations by revolving hydrometeor development processes around the production/distribution of graupel rather than using predictive equations (Hong and Lim 2006). The Thompson

TABLE 1. Times for which the ETSs for 6-hourly MCS rainfall and MAEs for LLJs were calculated. The exes (X) show the matched times for the forecast accuracy of the LLJ total, geostrophic, and ageostrophic wind magnitudes and direction, atmospheric water vapor content, and potential temperature, which were correlated with the MCS precipitation forecast skill.

Times (UTC)	ETS 0000–0600 UTC	ETS 0300–0900 UTC	ETS 0600–1200 UTC
MAE 0300	X	X	X
MAE 0600		X	X
MAE 0900			X

MP scheme (defined in Thompson et al. 2008) uses prognostic ice and rain number concentrations with time-split fall terms to determine hydrometeor evolution with time. To understand how PBL development might influence the LLJ and the correlation of forecast accuracy, three PBL schemes were utilized: the MYJ, MYNN 2.5, and YSU. The MYJ is a local scheme (MY 2.5 scheme revised) that uses a prognostic calculation for turbulence, with the addition of a viscous sublayer to the PBL through molecular diffusion (Janjić 1994). The local mixing-based MYNN 2.5 scheme uses a prognostic equation to calculate the turbulent kinetic energy in the boundary layer, but leaves thermodynamic variables as diagnostic in nature (Mellor and Yamada 1982; Nakanishi 2001). The YSU scheme is a nonlocal mixing scheme that evaluates the entrainment of air into the PBL mixed layer from above the inversion (Hong et al. 2006). With six WRF runs (configurations consisting of three PBL schemes under two MP schemes) per case for 31 cases, a total of 186 WRF runs compose the total model output in this experiment.

A Gaussian filter was applied to the WRF base variables before any data assimilation, regridding, or postprocessing were performed in order to eliminate atmospheric features with a wavelength less than $2\Delta x$ of the coarser RUC analyses (26 km) so that the environment could be evaluated on the scale of the RUC for a fair comparison when LLJ forecast accuracy was calculated.

Mean absolute error (MAE) was computed to measure the forecast accuracy between the 13-km RUC analyses and the 4-km WRF simulations for LLJ variables. The 4-km WRF output was regridded to the 13-km grid used in the RUC analyses, with a subdomain centered over the LLJ subjectively selected for LLJ MAE calculations (explained shortly). For determining the forecast accuracy of the LLJ, all grid points below the 65th percentile criteria for the magnitude of the total wind and with a northerly component were filtered out of the regridded WRF and RUC analysis outputs. The 65th percentile of the total wind was defined as the set of grid points with a southerly wind component, with the top 35% strongest wind speeds within a 250–2000 m AGL (at 250-m intervals) layer compared to the grid point with the strongest southerly wind (within 250–2000 m AGL) noted. This calculation was performed for both the RUC analysis and WRF, separately, for each case. Subjective analysis revealed that the 65th percentile captured the wind magnitudes that roughly fit the Bonner (1968) II–III criteria for nearly all of the LLJ cases in both the RUC and WRF (demonstrated in Figs. 8 and 10 below, but for the altitude of the low-level wind maximum only). The directional component of the LLJ total wind and directional and magnitude components of the ageostrophic and geostrophic winds, potential temperature, and atmospheric water vapor content were calculated only at the same points as the total wind magnitude (so that the MAEs of these variables were calculated in the LLJ exclusively). The MAE is defined as

$$\mathrm{MAE} = \frac{1}{n}\sum_{i=0}^{n} |X_i - Y_i|, \tag{1}$$

where n is the total number of grid points at or above the 65th percentile of the total wind magnitude in both the RUC and the WRF in a 250–2000-m (at 250-m intervals) layer, X is the WRF output at a given grid point i, and Y is the RUC analysis output at the same grid point i. The subdomains for which the LLJ variable MAEs were calculated were subjectively adjusted for the times calculated (0300, 0600, and 0900 UTC) to avoid convective contamination and resultant false responses in the MAEs and subsequent correlation calculations. Since MAE does not weigh outlier cases as heavily as the root-mean-square error (RMSE) and with the small sample size presented in this research, MAE was considered a reasonable bulk statistic for this experiment.

Stage IV 6-hourly precipitation observations (NCAR/UCAR/EOL 2015) from derived multisensor analyses (Lin and Mitchell 2005) were also regridded to the 4-km WRF domain and compared to forecast 6-hourly rainfall to determine the WRF precipitation forecast skill. The neighborhood ETS and frequency bias, defined in Clark et al. (2010), were chosen to evaluate the MCS precipitation forecast skill. Unlike traditional ETSs, which are calculated via contingency tables of forecast hits, misses, and false positives for each grid point, neighborhood calculations are derived by seeking out correctly forecasted hits within a given radius of influence. For each grid point, if the threshold of precipitation is correctly simulated within the radius of influence, that point will also be assigned a hit. This allows for simulations to be fairly recognized for their accuracy without heavy penalties given to fine horizontal grid-spaced forecasts with only a slight displacement error.

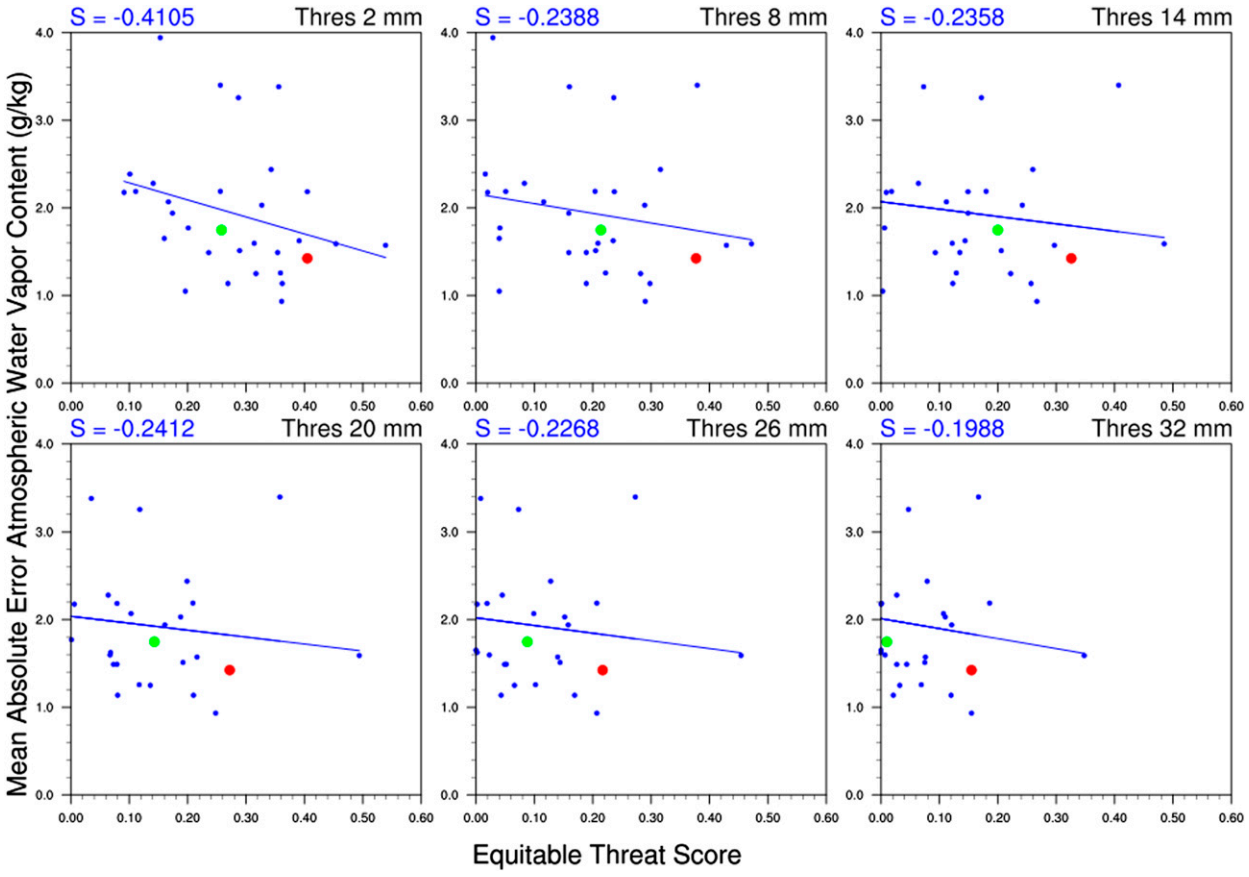

FIG. 4. Scatterplots demonstrating the correlation between the 0600–1200 UTC ETSs and 0900 UTC LLJ atmospheric water vapor content MAEs for the 2–32 mm at 6-mm interval ETS precipitation thresholds tested for the Thompson MYJ configuration. The plots show all 31 cases and their respective Spearman rank correlation coefficients, with a regression line added to demonstrate correlation behavior. The enlarged red and green markers represent the 24 May 2007 and 6 Jul 2011 cases, respectively.

Neighborhood ETSs were calculated at precipitation thresholds of 2.0–40.0 mm, at 2.0-mm intervals, for the entire WRF domain at 0000–0600, 0300–0900, and 0600–1200 UTC time periods in order to capture the evolution of precipitation during the developmental, mature, and dissipation stages of the MCSs. Similar to Clark et al. (2010), a radius of influence of 60 km was used to delineate the bounds of convection-allowing precipitation forecast skill, but without the punishment of small displacement errors in decent forecasts.

LLJ MAEs at 0300, 0600, and 0900 UTC were compared to ETS values during these three time periods to explore correlations during various LLJ and MCS stages (Table 1). It was mentioned by Mason (1989), Hamill (1999), and Mesinger (2008) that a model wet bias could artificially inflate the ETSs, diminishing the validity of using the ETS in such cases. As such, ETSs were evaluated with their associated frequency biases to explore if such behavior was present.

Given the relatively small sample size of type C and A LLJ regimes evaluated in this study, the Spearman rank correlation S was used to determine the magnitude of correlation between forecast accuracy of the LLJ (MAEs) and forecast skill of MCS precipitation (ETSs), both for the full sample as well as for just type C and type A cases separately. In Myers and Well (2003), S is defined as

$$S = 1 - \frac{6\sum_{i=1}^{n}(x_i - y_i)^2}{n(n^2 - 1)}, \tag{2}$$

where i represents each case out of n total number of samples and x_i and y_i are the ranks of the variables to be correlated. For the present research, x represents the ETS and y represents the MAE of the LLJ variable. While not a panacea to dealing with small sample sizes, the advantage to using the Spearman rank correlation is that it dampens the impact outlier cases have on correlated sets of data. In addition, the Spearman rank correlation is sign sensitive, which proved beneficial as negative correlations were what was desired for this

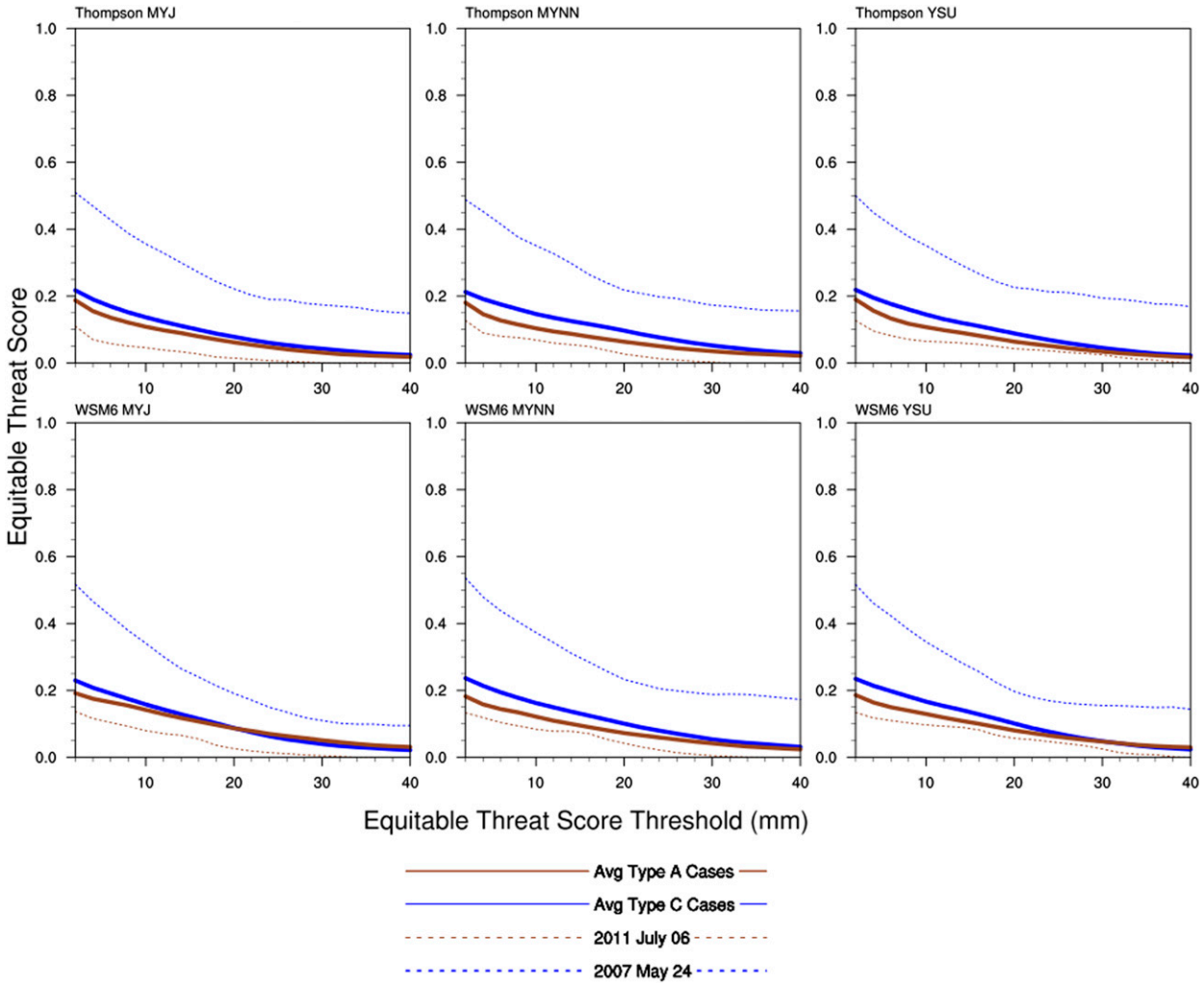

FIG. 5. ETSs for 6-h QPFs for all six WRF configurations for the 0000–0600 UTC period. Thresholds range from 2 to 40 mm at 2-mm intervals (x axis). Dashed blue and brown lines denote the 24 May 2007 type C and 6 Jul 2011 type A cases, while the heavy solid blue and brown lines represent averages of the type C and A cases, respectively.

research (where decreasing MAE for a sample of cases along the y axis correlated with increasing ETSs along the x axis). The Spearman rank correlation is also a nonparametric test, meaning one does not have to assume a particular data distribution. In this case, the LLJ variables and MCS precipitation are statistically independent of each other, deeming this statistic appropriate to use. As noted in Conover (1971), the Spearman rank correlation itself can also be used as a test statistic, including the two-tailed hypothesis test, which in this case takes into account whether higher ETSs could be paired with lower values of LLJ MAEs or vice versa. Using the 95th quantile of the Spearman rank correlation values, which varies based on the sample size of the correlating datasets, one can determine the threshold for statistical significance. Using Conover's (1971) Table A10, for sample sizes of 31, 16, and 15, corresponding to the sample sizes of all LLJ cases inclusive, as well as type C and A cases exclusively in this experiment, the critical threshold for the statistical significance of the Spearman rank correlations are $S = -0.2984$, -0.4265, and -0.4429, respectively. Using the 90th quantile for determining the statistical significance for all cases, as well as the type C and type A cases exclusively, Spearman rank correlations are $S = -0.2350$, -0.3382, and -0.3500, respectively.

Helland (1987) among others cautioned against trusting correlation values alone and advised graphical analysis for checking results. In the present study, scatterplots of LLJ MAEs versus MCS precipitation ETSs at a given threshold with a line of best fit were generated and evaluated to validate S results. Figure 4

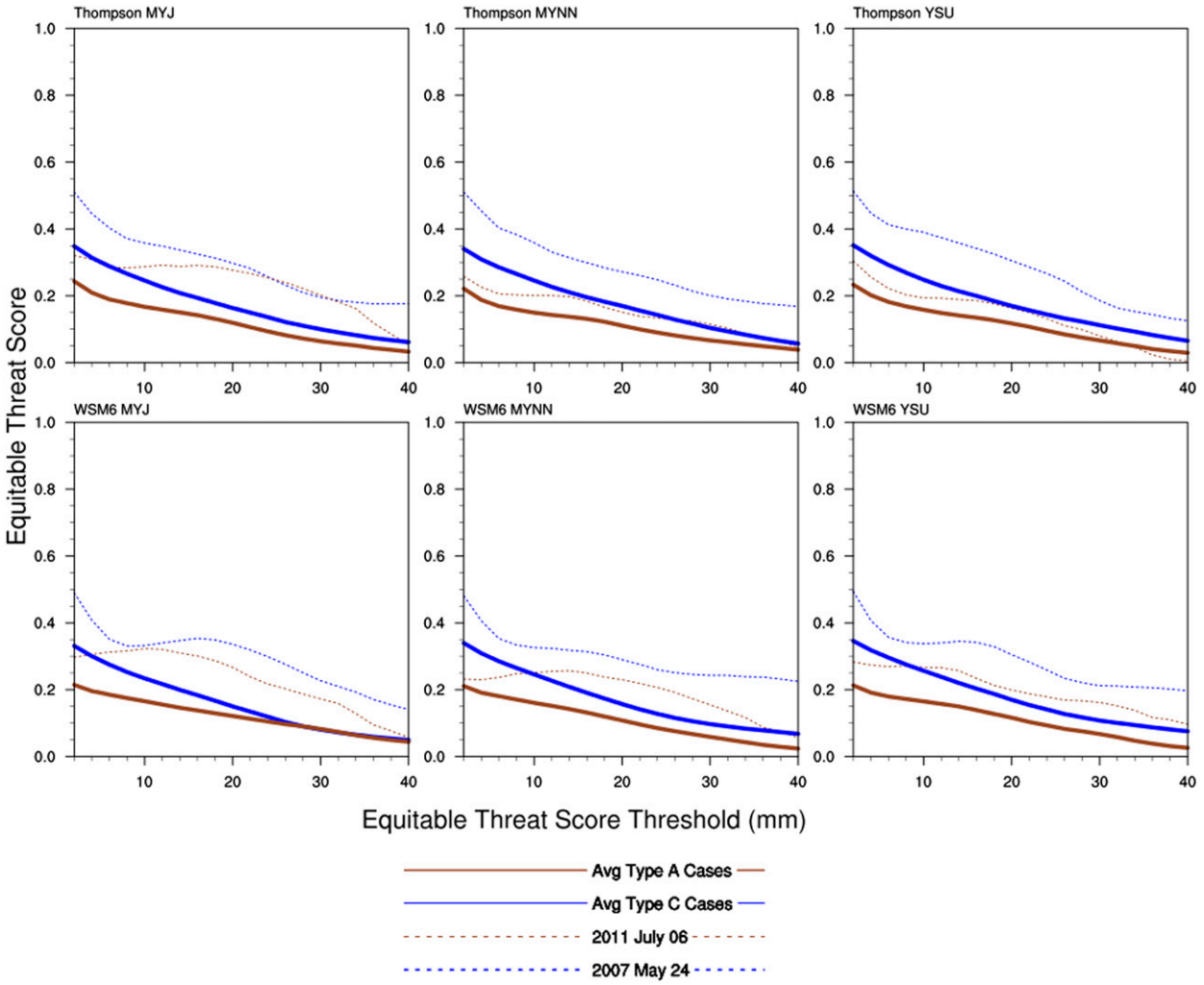

FIG. 6. As in Fig. 5, but for the 0300–0900 UTC period.

demonstrates the evolution of the correlations of 0600–1200 UTC ETSs and 0900 UTC atmospheric water vapor content MAEs with increasing ETS precipitation thresholds using the Thompson MYJ configuration. As the precipitation threshold increases, ETSs diminish in magnitude given that simulating smaller areas of heavier rainfall from convective cores with little error in timing or horizontal displacement still remains a difficult task, even with finer grid spacing with neighborhood-based forecast skill metrics. Increasing thresholds also shows greater variability for LLJ forecast accuracy and a decreased magnitude in the Spearman rank correlation, patterns of behavior noted between the MCS precipitation forecast skill and LLJ forecast accuracy of other variables at all other times tested. In Fig. 4, the 24 May 2007 and 6 July 2011 case points were highlighted for reference in section 3a.

It is important to note that correlation does not equal causation. Rather, S depicts a linear trend between the LLJ parameter forecast accuracy and MCS precipitation forecast skill, suggesting an association between both variables. As mentioned earlier, other meteorological features beyond LLJ characteristics play a role in supporting MCSs, possibly contributing to serial correlation effects. Spearman rank correlations for all WRF configurations were plotted on x–y-axis charts to determine the distance for which correlations between the LLJ parameter accuracy and MCS precipitation forecast skill were statistically significant across multiple ETS precipitation thresholds. For the plots, Spearman rank correlations were multiplied by -1 so that the magnitude of the results showing increasing MCS precipitation forecast skill with decreasing LLJ variable errors could be plotted along the positive x and y axes, providing for an easier read of the results.

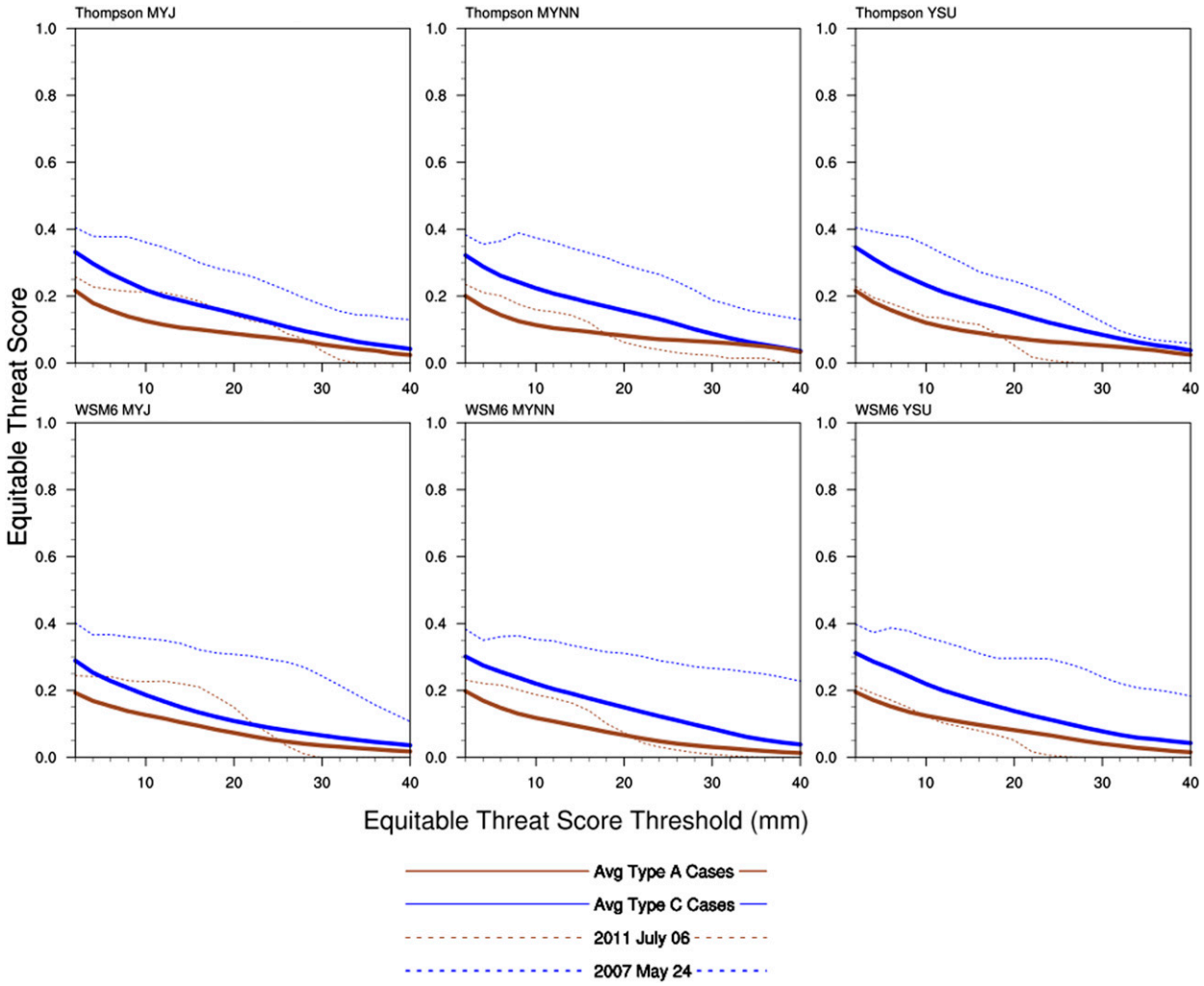

FIG. 7. As in Fig. 5, but for the 0600–1200 UTC period.

3. Results

a. Neighborhood ETS and bias

ETSs were lowest within the 0000–0600 UTC time frame (Fig. 5), with higher values more prevalent during the 0300–0900 UTC (Fig. 6) and 0600–1200 UTC (Fig. 7) periods. Among all three 6-h intervals for all six WRF configurations, type C cases exhibited better forecast skill compared to type A cases. Figure 8 demonstrates the forecast skill for one of the better predicted type C cases (the 24 May 2007 event) using the Thompson MP and MYJ PBL schemes. While some spatial and temporal displacements exist for heavier precipitation (60+ mm), the overall evolution of the MCS precipitation was captured well by the WRF (except for the Oklahoma extension of the MCS during the 0600–1200 UTC period). Employing the neighborhood approach with a radius of influence of 60 km, this forecast scored relatively well compared to the other cases (as demonstrated by the red marker in Fig. 4). Figure 9 shows the LLJ wind and moisture fields for 0300, 0600, and 0900 UTC, where the moisture fields were drier in the WRF than in the RUC analyses. The direction and magnitude of the wind fields were simulated with relative accuracy, as indicated by the contours representing the 65th percentile of the total wind field at the altitude of the low-level wind maximum (for this case, 750 m AGL). Despite the drier LLJ moisture profile in the WRF, a relatively good MCS precipitation forecast still resulted, suggesting that the forecast accuracy of the LLJ flow patterns may bear more importance than the moisture field. This case included a strong synoptic cold front, depicted with good agreement in all WRF configurations compared to the RUC analysis (not shown), providing large-scale lift, with strong forcing from other mechanisms beyond the LLJ

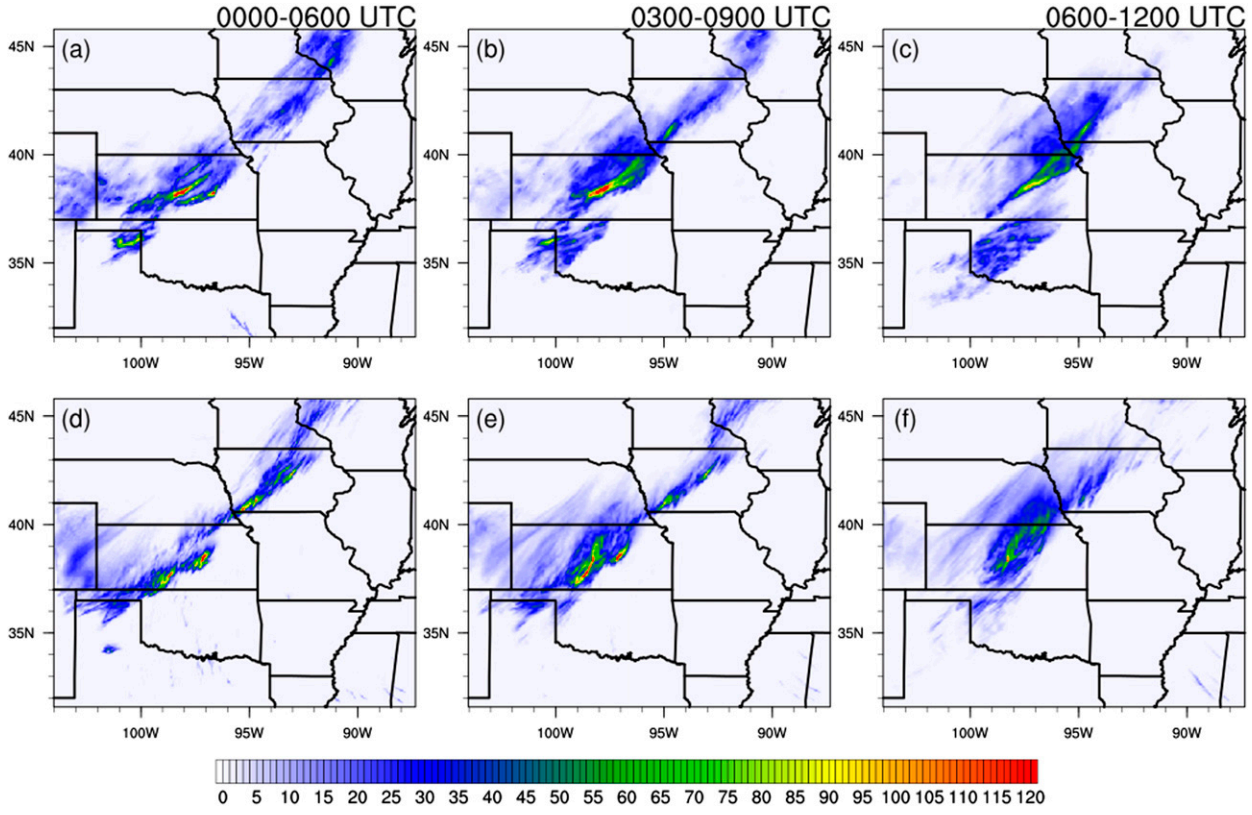

FIG. 8. Six-hourly precipitation (mm) for the 24 May 2007 type C case for (a)–(c) stage IV analysis and (d)–(f) Thompson MYJ WRF forecast precipitation. Results for the (left) 0000–0600, (center) 0300–0900, and (right) 0600–1200 UTC time periods.

playing important roles in MCS evolution. This was the case for most type C and a few type A events.

A less impressive forecast for a type A event (the 6 July 2011 event, represented by the green marker in Fig. 4 and the narrow brown dotted curve in Figs. 5–7) is shown in Fig. 10. The WRF-simulated LLJ for 0300, 0600, and 0900 UTC (Fig. 11) was quite shallow, weaker, and drier compared to the RUC analysis, where the 65th percentile of the total wind magnitude at the low-level wind maximum altitude (500 m AGL) at 0600 UTC indicated magnitudes up to $5\,m\,s^{-1}$ higher compared to the WRF. The WRF had an earlier simulation of the MCS compared to what was observed, with nearly 50 mm of precipitation accumulation during 0000–0600 UTC in central Nebraska (Fig. 10d) compared to almost nothing observed (Fig. 10a), with the MCS dissipation more notable in the 0600–1200 UTC time frame for the WRF (Fig. 10f) than in the observations (Fig. 10c). The earlier demise of the simulated MCS may have been due to less simulated atmospheric water vapor content and wind magnitude within the LLJ, where a drier and hence more stable atmosphere hindered the continuation of healthy MCS activity well into the 0600–1200 UTC time frame. In this case, no additional sources of strong forcing or upward ascent (such as a cold front) were present, possibly contributing to increased sensitivity between LLJ moisture forecast errors and errors in MCS precipitation. Determining the focus of convective initiation and features sustaining the MCS outside the LLJ with the absence of strong forcing mechanisms is a difficult forecast problem for type A LLJ-based regimes, a finding that concurs with Schumacher and Johnson (2009). Furthermore, uncertainty in the synoptic features and resultant errors in MCS forecasts was highlighted by Peters and Roebber (2014), demonstrating the need to further investigate large-scale relationships between forecast LLJ variables and MCS precipitation. Based on this case alone, one might hypothesize that forecasted MCSs in weakly forced LLJ regimes would be highly dependent on the atmospheric water vapor content provided within the LLJ to foster enough buoyancy for nocturnal convection to endure in an organized fashion. Forecast most unstable convective available potential energy (MUCAPE) and most unstable convective inhibition (MUCIN) profiles within the immediate vicinity of simulated MCSs along with gravity wave generation may also have a dominant influence on weakly forced MCS events such as the case

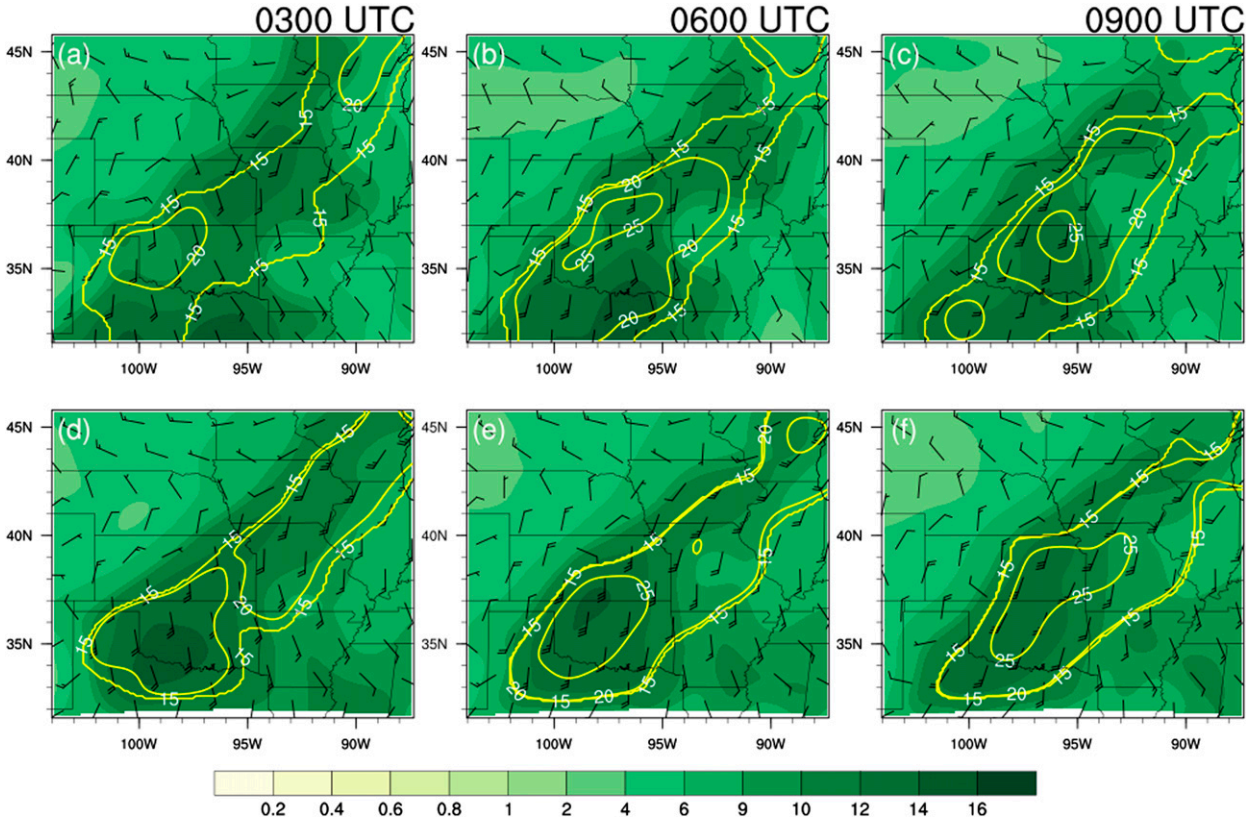

FIG. 9. Total wind (barbs in m s^{-1}, where each half barb is 5 m s^{-1}, and each full barb is 10 m s^{-1}), atmospheric water vapor content (filled contours in g kg^{-1}), and the 65th percentile of the total wind magnitude representing the LLJ (yellow line contours in m s^{-1}) plotted at the altitude of the low-level wind maximum (750 m AGL) for the 24 May 2007 type C case for the (a)–(c) 0-h 13-km RUC analysis and (d)–(f) Thompson MYJ WRF. Results for the (left) 0300, (center) 0600, and (right) 0900 UTC time periods.

currently discussed, but evaluation of these parameters extends beyond the scope of the current study.

The frequency bias (henceforth referred to as bias) was evaluated to determine what role it may have played on forecast skill measures for MCS precipitation with increasing ETS precipitation thresholds. Average biases were calculated by summing up the contingency table elements for type C or A cases and then calculating the bias as the final step. Outlier values of biases at higher precipitation thresholds often occurred with limited areal coverage so that they were given less weight via the averaging procedure. Figure 12 shows the weighted averaged biases for all WRF configurations for the 0300–0900 UTC period, with the blue and brown lines representing the averages of the type C and A cases, respectively. Similar trends existed for the 0000–0600 and 0600–1200 UTC periods (not shown). Figure 12 demonstrates that QPF biases are relatively small and thus should not have a significant impact on the results. Outlying biases for individual cases (not shown) for the higher precipitation thresholds in both type C and A LLJ cases were due to large spatial and timing errors in MCS precipitation. Figure 13 compares the 6-hourly observed precipitation to the WRF Thompson MYJ scheme precipitation for the 20 June 2010 case. During 0000–0600 UTC, a shorter-lived MCS occurred in Kansas (Fig. 13a), while at 0300–0900 UTC (Fig. 13e), Thompson MYJ depicted MCS precipitation in southwest Iowa. These timing and northward displacement errors were quite common, often resulting in higher biases in some cases for higher precipitation thresholds, especially for type A cases where the WRF (regardless of configuration) struggled to properly simulate MCSs in weakly forced synoptic regimes, particularly when a shallow, weak LLJ was present. Squitieri and Gallus (2016, manuscript submitted to *Wea. Forecasting*, hereafter Part II) investigated the northward displacement of the LLJ features and MCS precipitation based on the LLJ regime present in more detail.

Nocturnal LLJ and associated MCS environments differ from each other to the extent in which the LLJ and MCS precipitation relationship becomes obscured by other meteorological factors, such as additional forcing mechanisms. While a general association

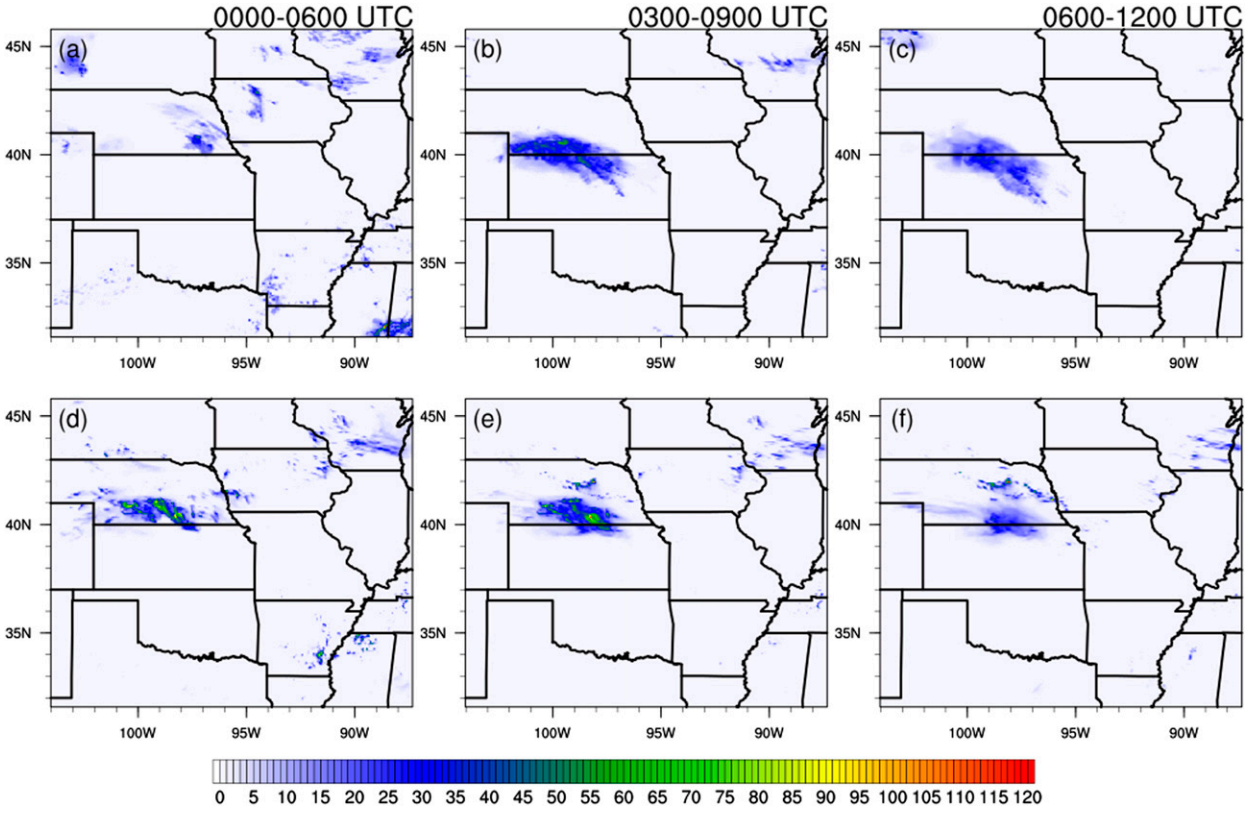

FIG. 10. As in Fig. 8, but for the 6 Jul 2011 type A case.

between LLJ and MCS evolution can be made, it is important to differentiate between strongly and weakly forced synoptic LLJ environments in order to gauge the significance of the role the LLJ may play in initiating and sustaining nocturnal convection. Evaluating the characteristics of the LLJ itself (i.e., height, time and magnitude of the peak wind, and LLJ depth) is also important, especially when the LLJ becomes the main forcing mechanism for nocturnal convection (discussed in Part II).

b. *Correlation of the forecast accuracy of LLJ variables with forecast skill of MCS precipitation*

No significant correlations were found between the forecast accuracy of the total, geostrophic, or ageostrophic wind magnitudes (not shown) within the LLJ and forecast skill of the MCS precipitation in the WRF. For the accuracy of the LLJ total wind direction at 0300 UTC versus the forecast skill of the MCS precipitation from 0000 to 0600 UTC, statistically significant correlations existed (Fig. 14). Across most of the ETS precipitation thresholds tested (mainly below 30 mm) for all WRF configurations, statistical significance was widespread when considering the full sample of cases at both the 95% and 90% thresholds of confidence for rejecting the null hypothesis. For type C cases, statistical significance at the 90% threshold was present for the Thompson MYJ, Thompson MYNN, and Thompson YSU runs for nearly all ETS precipitation thresholds tested. At the 90% confidence interval for significance, for the 2–14-mm ETS precipitation thresholds, statistically significant correlations were noted with the Thompson YSU and WSM6 MYJ configurations for type A cases. Occasionally significant correlations with the 90% confidence interval were seen with higher ETS thresholds for the Thompson and WSM6 MYNN runs as well. For the relationships between 0300 and 0900 UTC MCS precipitation forecast skill and the 0300 and 0600 UTC LLJ total wind direction forecast accuracy, as well as the 0600–1200 UTC MCS precipitation forecast skill and 0300, 0600, and 0900 UTC LLJ total wind direction forecast accuracy, statistically significant correlations were noted among most WRF configurations, across most ETS precipitation thresholds tested for type C cases alone and for the full set of all cases, especially above the 90% confidence interval for significance (not shown). No other significant correlations among type A cases were noted. It follows that the forecast orientation of the LLJ through all stages of the LLJ evolution

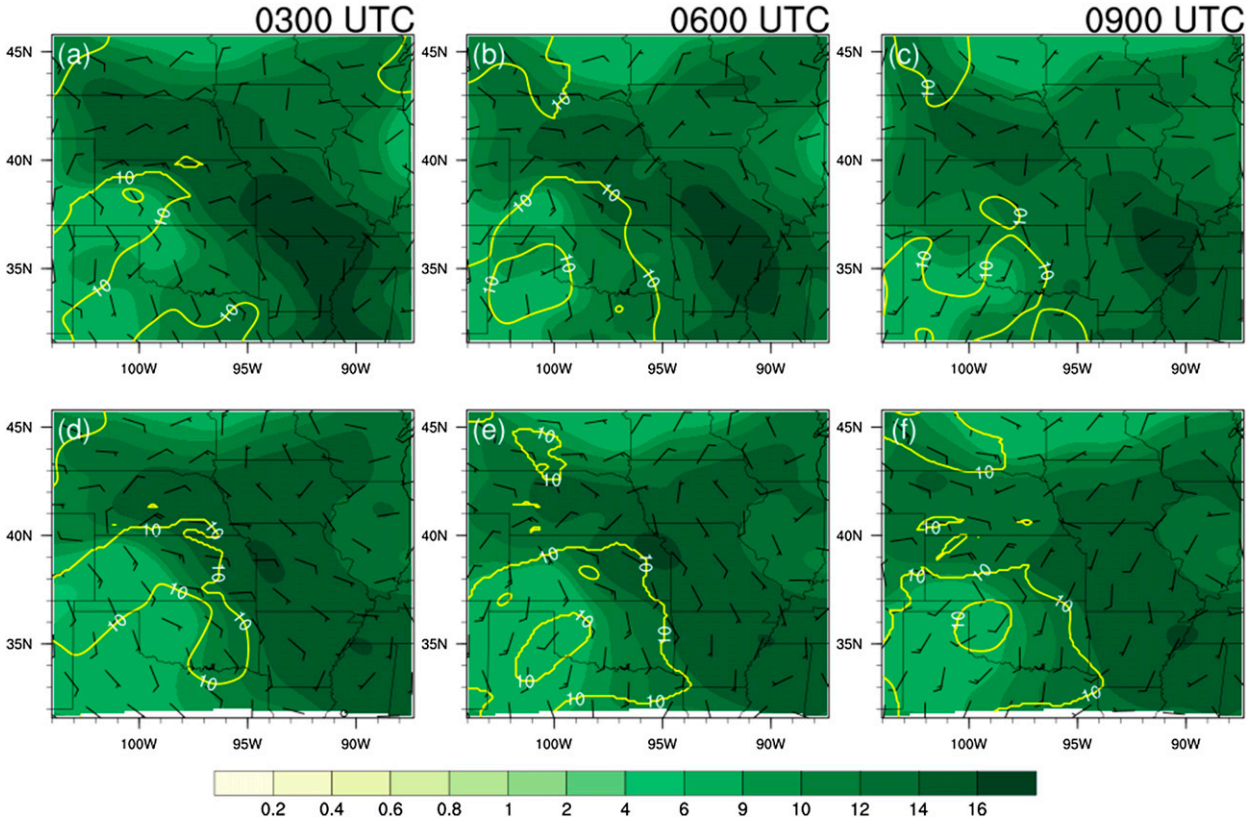

FIG. 11. As in Fig. 9, but for the 6 Jul 2011 type A case, with the low-level wind maximum observed at 500 m AGL.

is important in getting accurate QPFs during MCS evolution, especially for strongly forced regimes.

Statistical significance at the 95% confidence interval between geostrophic wind direction forecast accuracy at 0300 UTC and forecast skill of MCS precipitation at ETS thresholds mainly below 30 mm for the 0000–0600 UTC period was evident in all but the Thompson MYNN and WSM6 MYJ configurations for all cases inclusive (Fig. 15). At the 90% confidence interval for statistical significance, the WSM6 MYJ runs showed significance for all ETS precipitation thresholds below 28 mm, with the Thompson MYNN scheme demonstrating significance between the 12–28-mm ETS thresholds. Statistical significance was less prevalent for type C cases alone, where significance was demonstrated mainly above the 90% confidence interval for rejecting the null hypothesis up to approximately the 20-mm ETS precipitation threshold for all WRF configurations, though the significance among the Thompson schemes was marginal. For the 20–30-mm ETS thresholds, the Thompson YSU and WSM6 MYNN runs ceased to demonstrate significance, with the remaining WRF configurations behaving similarly past the 30-mm ETS threshold. For correlations between 0300 and 0900 UTC MCS QPF forecast skill and 0300 and 0600 UTC LLJ geostrophic wind direction forecast accuracy, as well as correlations between 0600 and 1200 UTC MCS QPF forecast skill and 0300, 0600, and 0900 UTC LLJ geostrophic wind direction forecast accuracy, statistical significance was sparse (not shown). A small exception existed for a few WRF configurations when considering all cases, or subsets of type C cases, and type A cases, where occasional significance below the 10-mm ETS precipitation threshold at the 90% confidence interval was noted. The developing LLJ background flow established by the orientation of the geostrophic wind field is important for determining the structure of the forecast LLJ (Augustine and Caracena 1994) and the location of its terminus, which impacts the timing and placement accuracy of the forecast MCS initiation and upscale growth. After the early stages of LLJ and MCS development, LLJ geostrophic wind direction forecasts did not strongly impact the forecast MCS evolution.

For the 0300–0900 and 0600–1200 UTC periods, MCS precipitation forecast skill significantly correlated with 0300 UTC ageostrophic wind direction forecast accuracy, mainly for type C cases among the WSM6 MYJ and YSU WRF runs for nearly all ETS thresholds tested, above the 95% confidence interval for significance (with

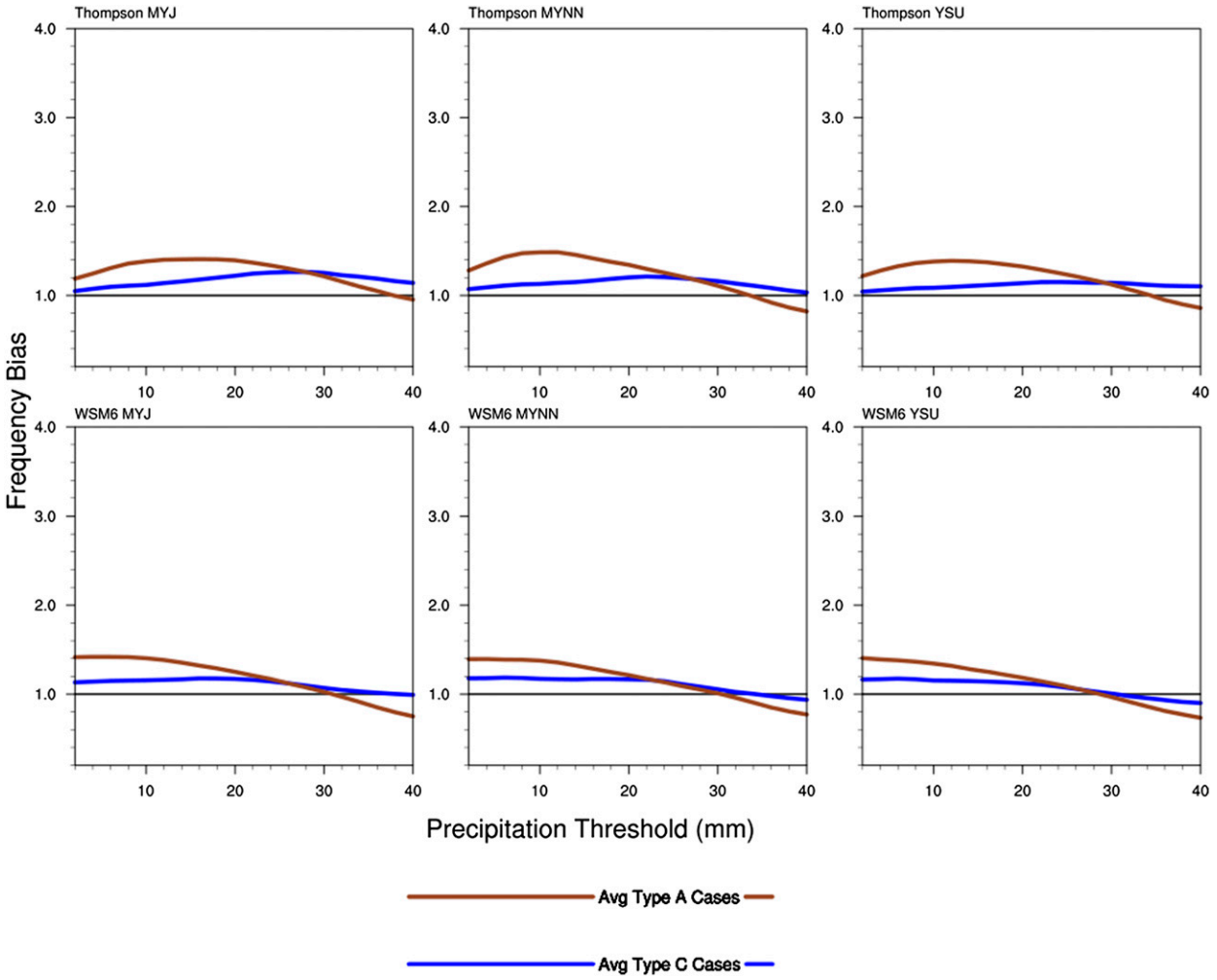

FIG. 12. The 6-h QPF biases for all six WRF configurations for the 0300–0900 UTC period. Precipitation thresholds range from 2 to 40 mm at 2-mm intervals (*x* axis). Solid blue and brown lines represent averages of the type C and A cases, respectively. The solid black line represents a bias of 1, indicating no bias error.

the 0300–0900 UTC period shown in Fig. 16). For all cases, mainly above the 10-mm ETS precipitation threshold at the 95% confidence interval, the WSM6 MYJ and YSU configurations demonstrated statistically significant correlations between 6-h MCS QPF and LLJ geostrophic wind direction forecast accuracy. The WRF configurations tested largely agreed on there being no significant correlations between LLJ ageostrophic wind direction forecast accuracy and MCS QPF forecast skill for type A cases. A difference in significance regarding correlations between Thompson versus WSM6 runs is noted and will be discussed later. The ageostrophic wind of the developing LLJ has a strong influence on mature MCS evolution both in all cases tested and for strongly forced regimes, as the timing and placement of the ongoing MCS will depend heavily on the accuracy of the convergence associated with the developing LLJ terminus and the associated impact on the skill of forecast MCS development time and location.

Significant correlations between atmospheric water vapor forecast accuracy at 0600 and 0300–0900 UTC (Fig. 17) and 0600–1200 UTC (not shown) MCS QPF forecast skill were noted, mainly for the full sample of cases and for the subset of type C cases. For the full sample, at 0300–0900 UTC and above the 90% confidence interval, all WRF configurations demonstrated statistical significance, at least to the 26-mm ETS precipitation threshold (where significance deteriorated for the Thompson MYNN runs). All but the Thompson MYNN runs were statistically significant up to the 20-mm ETS precipitation threshold for the 95% confidence interval for significance. Similar behavior of the correlations between 0300–0600 UTC MCS QPF forecast skill and 0600 UTC LLJ atmospheric water vapor

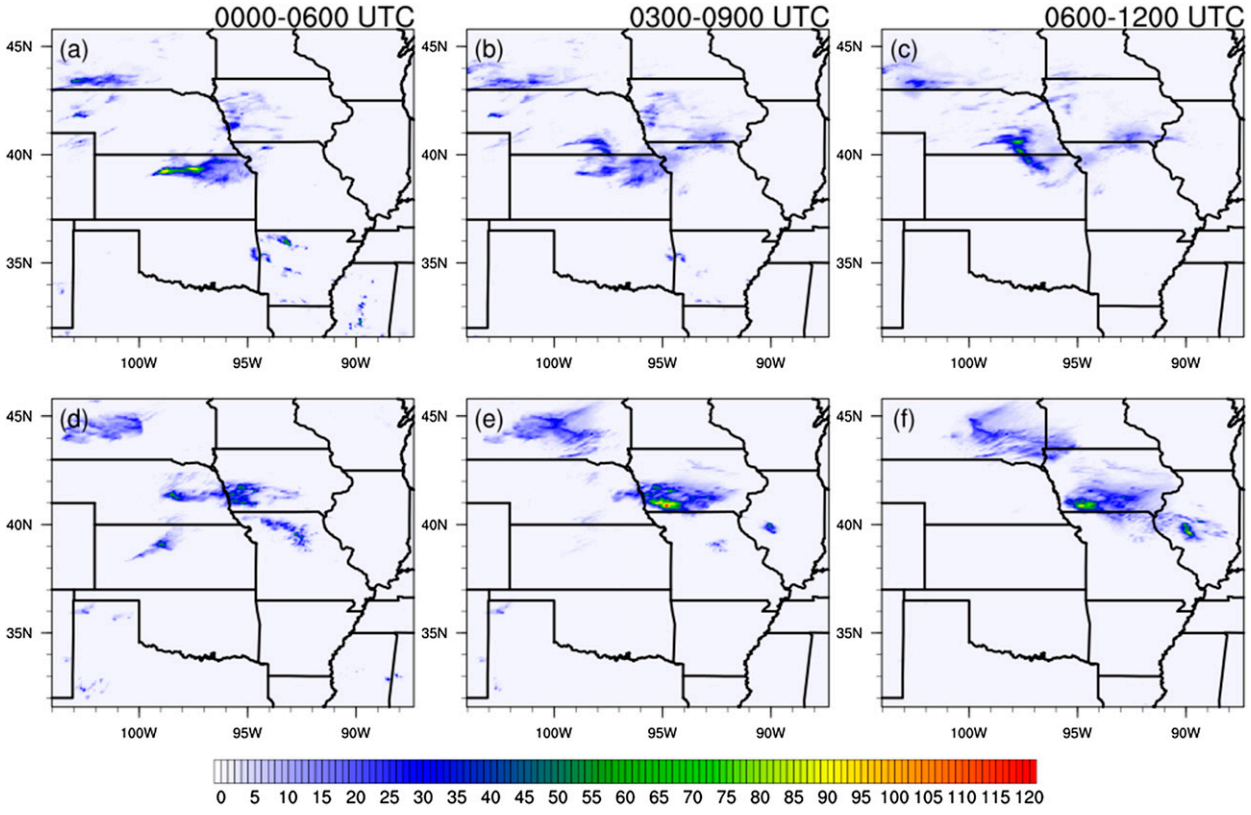

FIG. 13. As in Fig. 8, but for the 20 Jun 2010 type A case.

content forecast accuracy was noted for type C cases, but with more disagreement among the WRF configurations, and with less significant correlations across all ETS thresholds, especially for the Thompson, WSM6 MYNN, and Thompson YSU runs. As with previous LLJ variables tested, there are no significant correlations between LLJ moisture forecast accuracy and MCS QPF forecast skill for type A cases. Similar to the moisture content, the forecast accuracy of the mature LLJ potential temperature field significantly correlated to mature MCS QPF forecast skill. Specifically, 0300–0900 UTC MCS QPF forecast skill significantly correlated to the 0600 UTC LLJ potential temperature forecast accuracy, with both the 0600 and 0900 UTC (Fig. 18) LLJ potential temperature forecast accuracy results significantly correlating to 0600–1200 UTC MCS QPF forecast skill for the full sample of cases and the subset of type C cases, especially when considering Spearman rank correlations above the 90% confidence interval for significance. As noted with previous LLJ variables, a difference existed between the WSM6 and Thompson configurations, where the WSM6 runs were significantly correlated for nearly all ETS precipitation thresholds, with the Thompson runs demonstrating less correlation between LLJ potential temperature forecast accuracy and mature MCS QPF forecast skill, with no significance noted. This was not the case, however, for type C cases alone, and the reasons for this are unclear. Similar results were also noted for the 0300–0900 UTC ETS and 0600 UTC MAE, as well as the 0600–1200 UTC ETS and 0600 UTC MAE correlations. It follows that later in the LLJ and MCS evolution stages, the thermodynamic characteristics of the forecast LLJ air parcels become increasingly important for satisfactorily simulating the MCS precipitation. While sensitivity exists between the forecast LLJ orientation and MCS QPF throughout the evolution of the LLJ and MCSs, forecast LLJ thermodynamic characteristics become increasingly important later in the evening, even for strongly forced cases, where LLJ potential temperature forecast accuracy correlates more with MCS QPF forecast skill as the evening progresses (Fig. 19). It is suspected that waning instability due to diurnal cooling begins to have a bigger impact on MCS longevity during the late evening hours, when correctly simulating the thermodynamic properties of the LLJ will have a more significant impact on the accuracy of the forecast MCS evolution.

The sensitivity of the MCS QPF skill to multiple LLJ parameters varies between the LLJ types; thus, it can

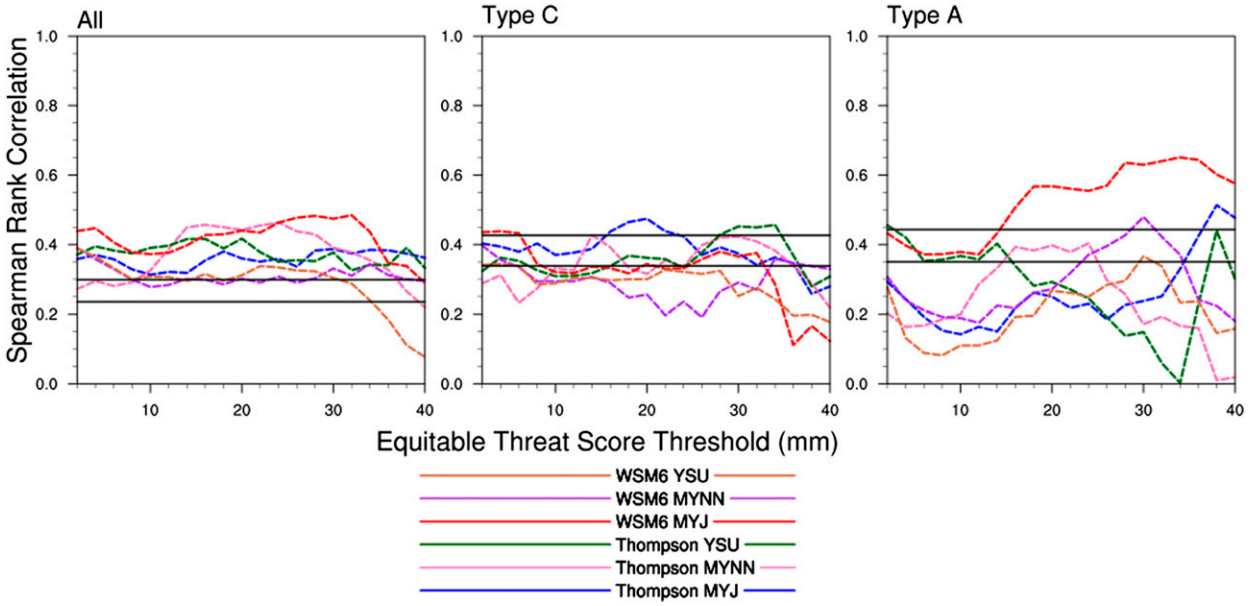

FIG. 14. Spearman rank correlations between the 6-h MCS QPF ETSs for the 2–40-mm thresholds at 0000–0600 UTC and the MAEs for the LLJ total wind direction at 0300 UTC, including all WRF configurations (colored dashed lines) for (left) the full sample of cases, (center) type C cases, and (right) type A cases. The top black line delineates the statistically significant Spearman rank correlation value as a function of sample size at the 95% confidence interval of rejecting the null hypothesis as defined in Conover (1971). The bottom black line is for the 90% confidence interval.

be misleading at times to consider the entire sample as a whole. Correlating 0600 UTC LLJ moisture forecast accuracy with 0300–0900 UTC QPF forecast skill at the 24-mm threshold for example, Fig. 20 shows that type C correlations are higher compared to type A events, where the LLJ moisture forecast accuracy and MCS precipitation forecast skill were poorer overall. The better correlations with type C cases likely influences the results for the entire set of cases sampled, an observation made repeatedly for numerous MCS precipitation forecast skill and LLJ forecast accuracy correlations during multiple time periods, under

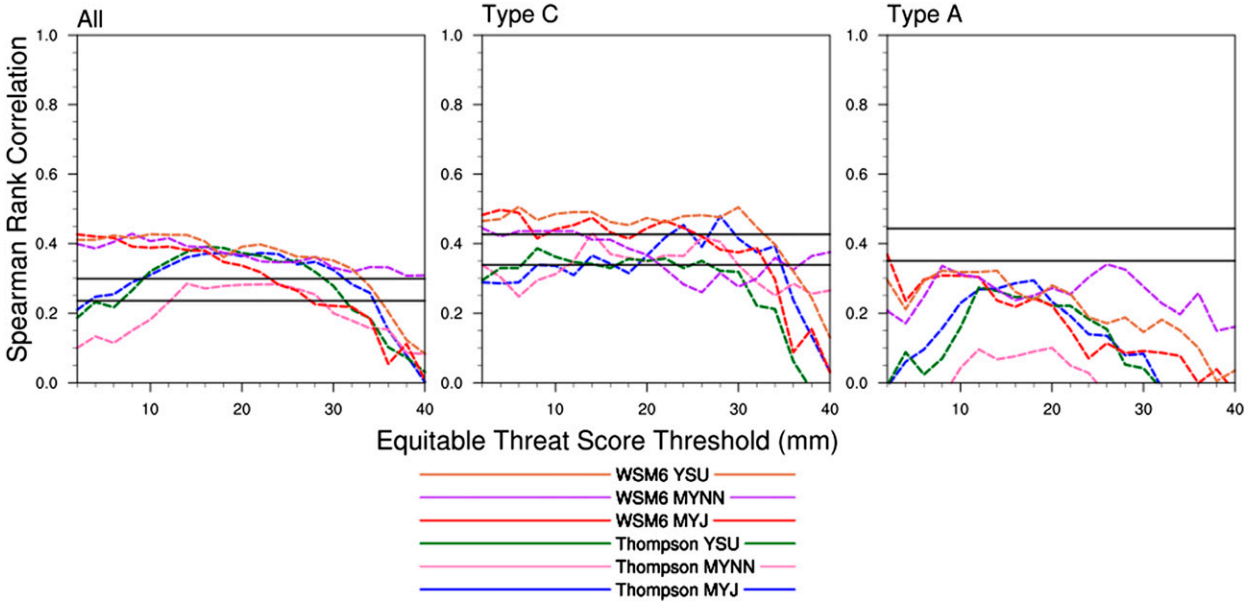

FIG. 15. As in Fig. 14, but for the LLJ geostrophic wind direction.

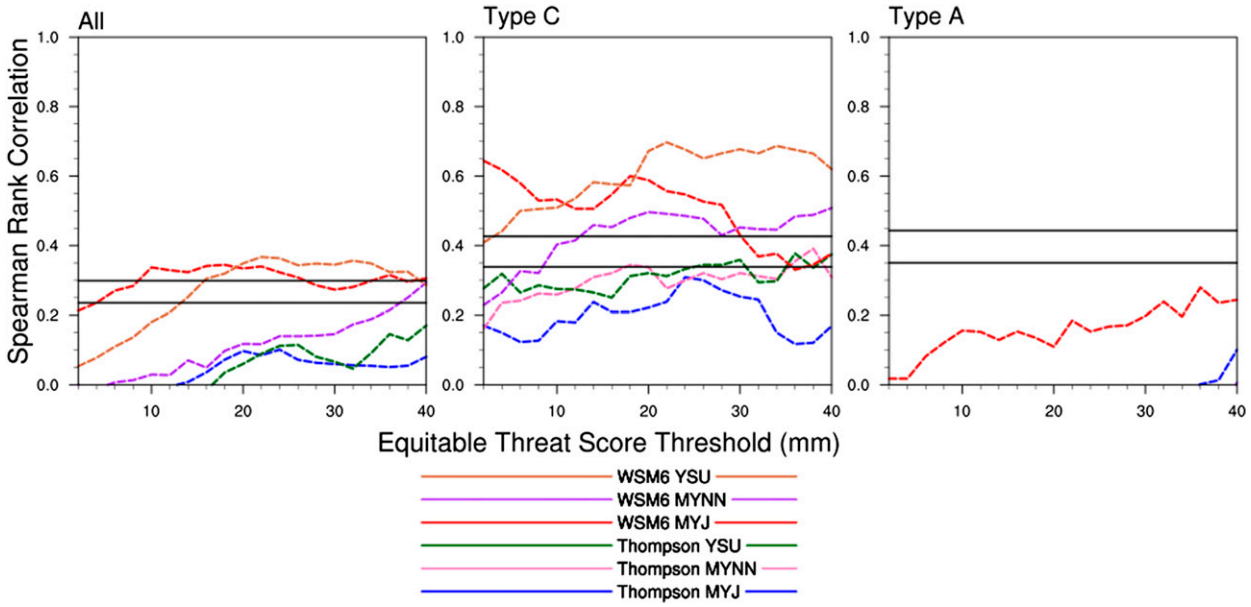

FIG. 16. As in Fig. 14, but for Spearman rank correlations between the 6-h MCS QPF ETSs for 2–40-mm thresholds at 0300–0900 UTC and MAEs for the LLJ ageostrophic wind direction at 0300 UTC.

multiple WRF configurations. The sensitivity of MCS QPF skill to the accuracy of forecasts of non-LLJ atmospheric features may also vary, further contributing to the complexity in the LLJ–MCS relationship, especially for type A cases, where focal mechanisms for convection are on smaller scales and are more ambiguous in nature. A review of the correlations of forecast accuracy of non-LLJ parameters such as MUCAPE and MUCIN to MCS precipitation forecast skill would thus be necessary, but is beyond the scope of this paper. In addition, the lack of significant correlations between the LLJ forecast accuracy and MCS precipitation forecast skill for weakly forced regimes requires more research. Unlike strongly forced LLJs, which occur in

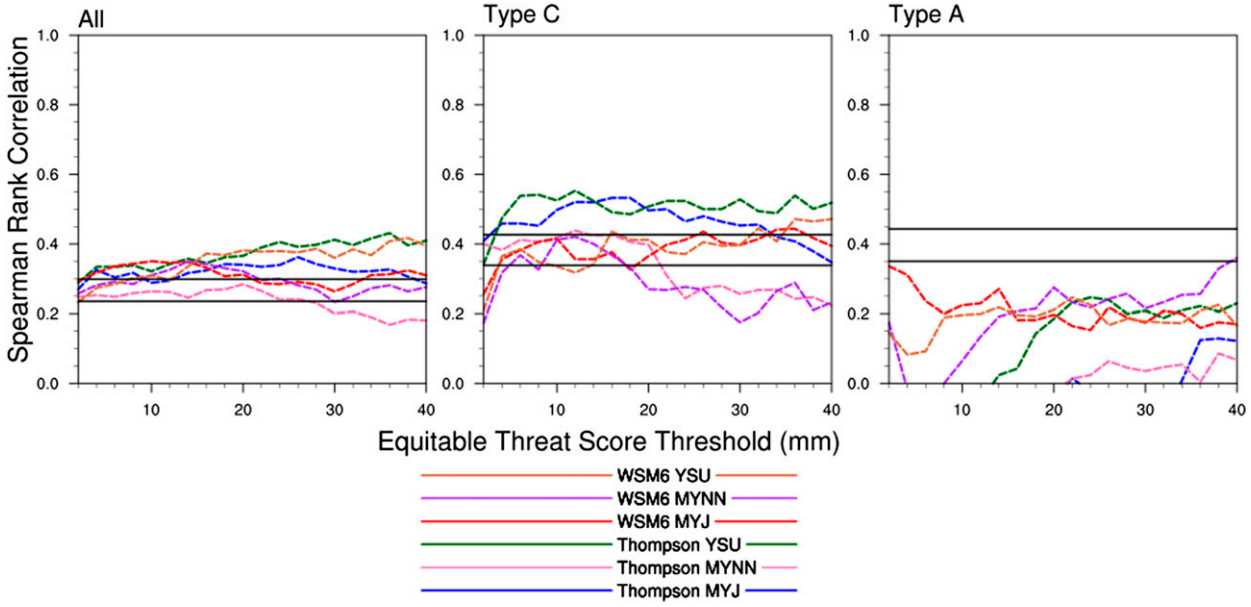

FIG. 17. As in Fig. 14, but with Spearman rank correlations between the 6-h MCS QPF ETSs for 2–40-mm thresholds at 0300–0900 UTC and MAEs for the LLJ atmospheric water vapor content at 0600 UTC.

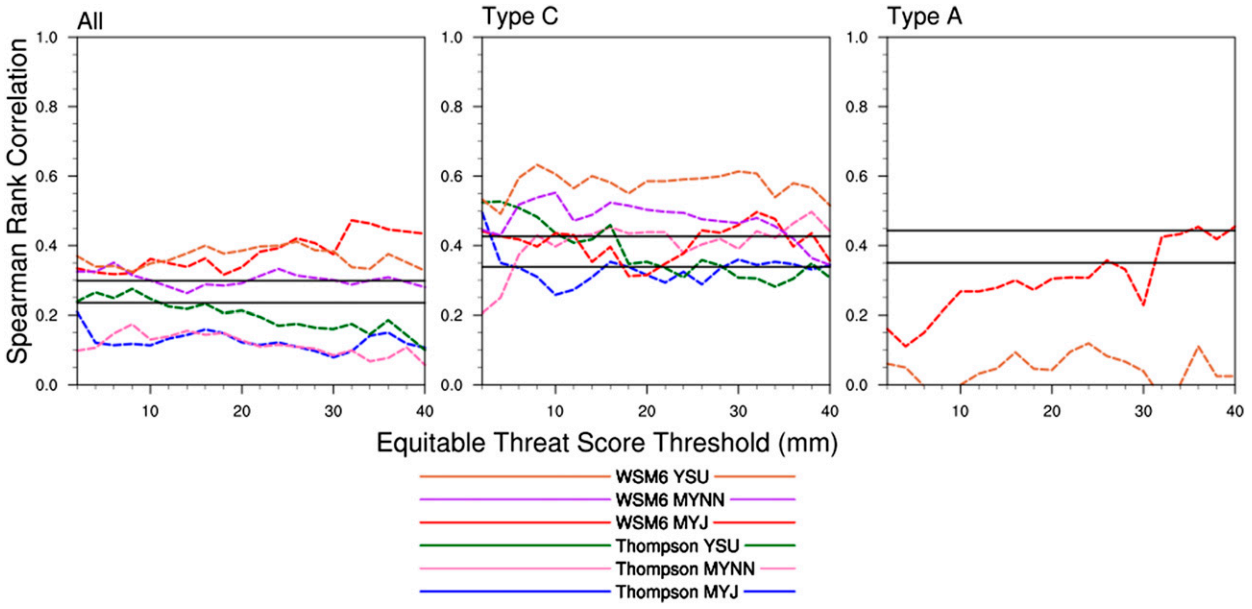

FIG. 18. As in Fig. 14, but with Spearman rank correlations between the 6-h MCS QPF ETSs for 2–40-mm thresholds at 0600–1200 UTC and the LLJ potential temperature at 0900 UTC.

regimes of strong forcing over broad areas and with similar synoptic features (such as upper and lower jet stream coupling and lee cyclogenesis), type A LLJ regimes are weakly forced and the LLJs are driven primarily by the inertial oscillation. Most importantly, type A regime MCSs, while fueled by the LLJ, are often initiated and sustained by smaller-scale features such as fronts and boundaries (Schumacher and Johnson 2009) at the mesoalpha or even mesobeta scales. Similarly, convection over the higher terrain of the high plains may trigger deep, tropospheric gravity waves, which may also be responsible for MCS evolution (Mapes et al. 2003; Schumacher 2009), thus impacting the timing of the MCS initiation and placement in simulations. Calculating bulk statistics such as the MAEs over the entire region of the LLJ may smooth these finer-scale features, introducing several inconsistencies within the type A regime

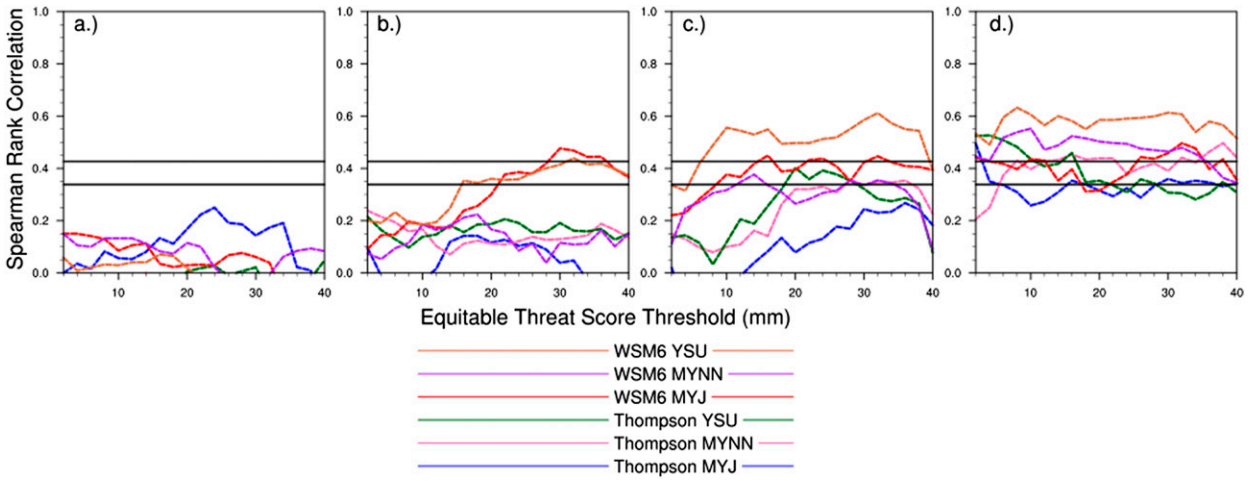

FIG. 19. As in Fig. 14, but for type C cases only, correlating (a) 0000–0600 UTC 6-h MCS QPF ETSs with 0300 UTC LLJ potential temperature MAEs, (b) 0300–0900 UTC 6-h MCS QPF ETSs with 0600 UTC LLJ potential temperature MAEs, (c) 0600–1200 UTC 6-h MCS QPF ETSs with 0600 UTC LLJ potential temperature MAEs, and (d) 0600–1200 UTC 6-h MCS QPF ETSs with 0900 UTC LLJ potential temperature MAEs.

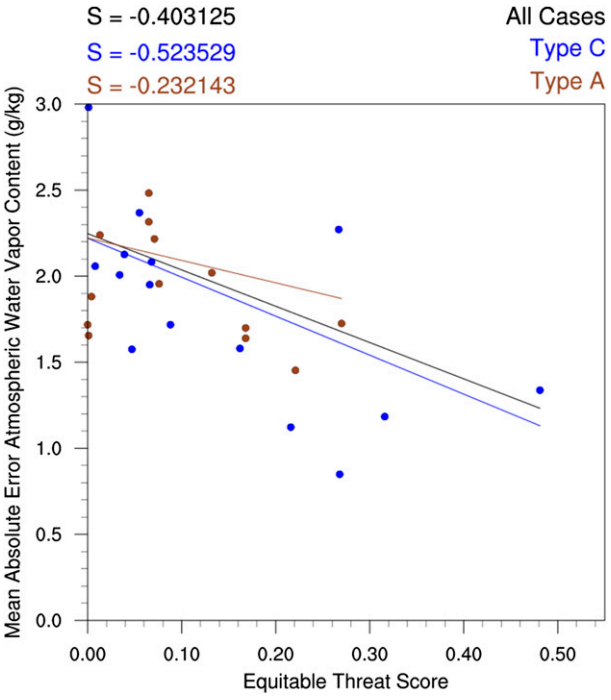

FIG. 20. Scatterplot demonstrating correlations between 0300–0900 UTC MCS QPF ETSs (at the 24-mm threshold) and 0600 UTC forecast LLJ moisture MAEs using the Thompson YSU configuration. The trend lines and Spearman rank correlations for the total set of cases (black), type C case subset (blue), and type A subset (brown) are included, with the type C and A subsets differentiated in color from the total case set.

datasets, yielding the weaker LLJ–MCS Spearman rank correlations. Duda and Gallus (2013) also found that the forecast MCS evolution was poorer in weakly forced environments compared to stronger forced events when evaluating cases using bulk metrics (i.e., ETS and FSS) for evaluating precipitation forecast skill.

Another concern is the variability in Spearman rank correlations over the range of ETS precipitation thresholds tested among the different WRF configurations. Some WRF configurations suggest statistical significance while other configurations do not. Specifically, the Thompson and WSM6 configurations often disagree (seen in Figs. 16 and 18). This can be seen, for instance, in Fig. 18 for all cases, where the WSM6 MYJ configuration Spearman rank correlations between the 0900 UTC LLJ potential temperature forecast accuracy and 0600–1200 UTC MCS QPF forecast skill were higher in magnitude and showed statistical significance while the Thompson MYJ correlations were weaker and showed no significance. Higher variability between all cases under the Thompson MYJ configuration (and thus weaker Spearman rank correlations) existed partly because of outlier cases, particularly at higher precipitation thresholds. Greater potential temperature MAEs for multiple Thompson MYJ runs compared to WSM6 MYJ forecasts exist across a greater span of ETSs, which is especially evident in the 20–32-mm threshold plots (Fig. 21). This greater variability in the Thompson MYJ runs versus the WSM6 MYJ results is likely what is causing the lower Spearman rank correlation values for Thompson MYJ. It is suspected that the level of simultaneous variability in both LLJ forecast accuracy and MCS QPF forecast skill between cases under different WRF configurations is responsible for the differences in correlations among the different configurations. Specifically, it appears that ETS values for WSM6 runs decrease much faster with respect to increasing precipitation thresholds than those for the Thompson runs. Similar behavior was noticed in the correlations of several other LLJ parameters to MCS 6-h QPF forecast skill. The choice of model PBL and MP schemes for forecasts is thus not a trivial one and more research into their impact on forecasts is needed (Weisman et al. 2008; Bryan and Morrison 2012; Adams-Selin et al. 2013). Future work is needed to answer questions relating to MP sensitivities and PBL interactions with nocturnal MCS evolution.

4. Conclusions and discussion

LLJ-induced MCS cases were divided between strongly and weakly forced synoptic regimes (types C and A, respectively). ETSs across all precipitation thresholds and WRF configurations in the 0000–0600 UTC time period showed less forecast skill than in the 0600–1200 UTC period, as the models struggled with the timing of convective initiation and upscale growth. Type C cases tended to have higher ETS values overall than type A cases since models handled the timing and placement of convective precipitation better in environments where stronger forcing prevailed. Environments with weaker forcing, more likely with type A cases, are more ambiguous regarding their sources of large-scale vertical ascent, providing a greater challenge for forecasters and model simulations alike (Jankov and Gallus 2004; Duda and Gallus 2013). As such, displacement errors were more prevalent in type A cases, leading to higher biases across most precipitation thresholds compared to type C environments.

The forecast accuracy of the LLJ total wind direction throughout the nocturnal period was commonly correlated with MCS QPF forecast skill for all 6-h periods studied, for the full sample of cases, and for the subset of strongly forced cases. It is unclear why stronger correlations between the LLJ and MCS QPFs were not present for weakly forced cases. A proposed theory is

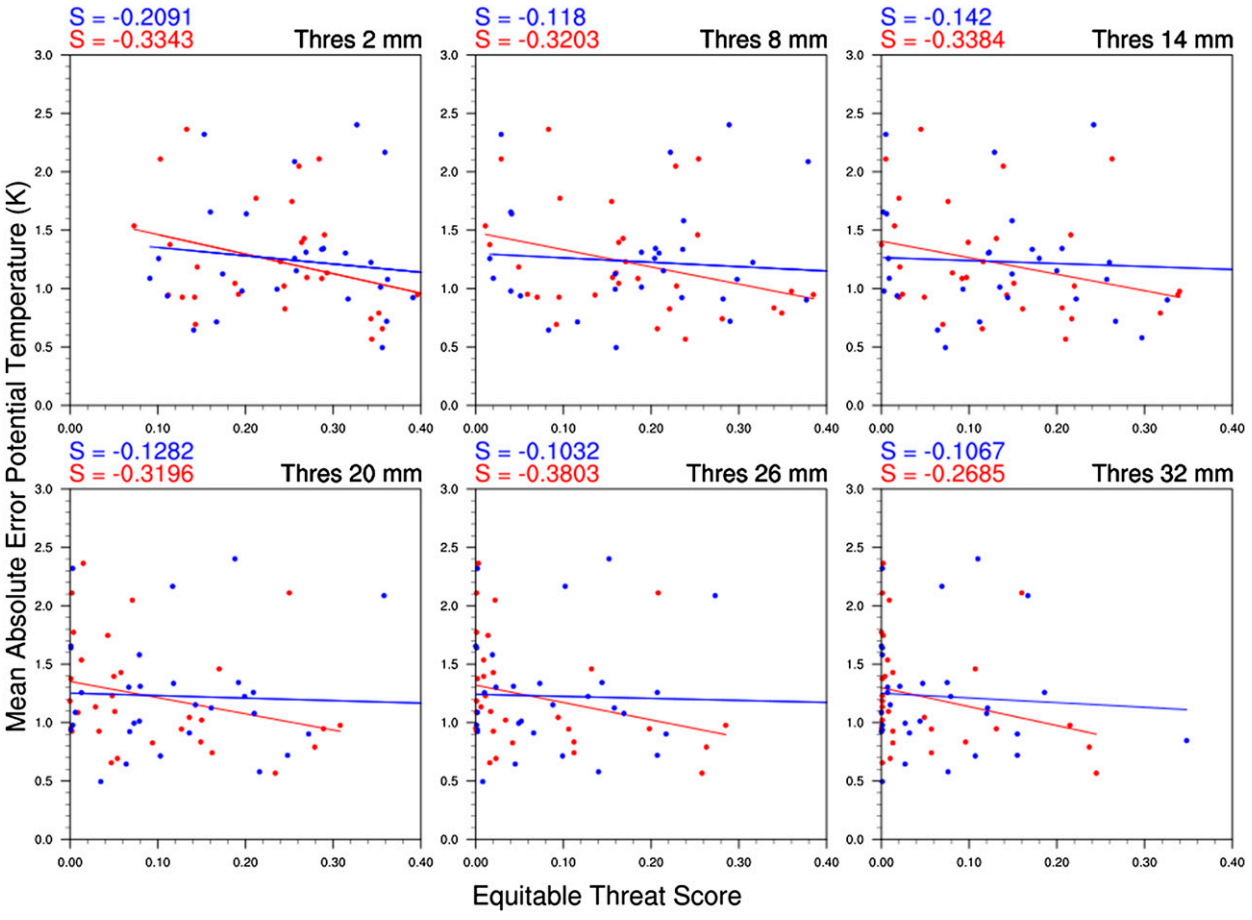

FIG. 21. Scatterplots differentiating the behavior of the Thompson MYJ (blue) and WSM6 MYJ (red) Spearman rank correlations for the 0600–1200 UTC MCS precipitation ETSs vs the 0900 UTC potential temperature MAEs for all cases inclusive, displayed in Fig. 18, for 2–32 mm at 6-mm interval ETS precipitation thresholds.

that the forcing mechanisms for initiating and sustaining convection in these environments vary greatly from case to case, occurring at small scales. Ambiguity is thus likely introduced when bulk statistics (which smooth over important details) are employed, hence the weaker correlations for type A cases. Forecast accuracy of the developing LLJ geostrophic wind orientation also showed a substantial association with developing MCS QPF skill, though the geostrophic wind orientation at later times did not significantly correlate to mature MCS QPF skill. The geostrophic wind provides the background profile upon which the LLJ builds, and the LLJ total wind acts as a key player in sustaining nocturnal convection (Cotton et al. 1989; Augustine and Caracena 1994; Mitchell et al. 1995; Higgins et al. 1997; French and Parker 2010). Accurately simulating the developing LLJ geostrophic wind direction is vital for understanding the early stages of forecast LLJ orientation and the resultant placement for key features that would contribute to MCS initiation and maintenance. The importance of these individual components varies between earlier season events with strong synoptic forcing and later summer events with weaker forcing. As such, it is important to evaluate the importance of all LLJ components separately for both regimes.

Within stronger forced environments, greater sensitivity was noted to dynamic and kinematic fields of the developing low-level jet stream, where statistical significance was noted with the correlations between the forecast accuracy of the LLJ ageostrophic wind direction early in the evening and the MCS precipitation forecast skill during the development stages of MCS evolution. The ageostrophic wind direction dictates the nature of convergent flow and rising motion along the LLJ terminus and along large-scale boundaries or fronts associated with dynamic synoptic regimes, particularly at the mesoscale (Markowski and Richardson 2010). In this case, the ageostrophic wind direction during the development stages of the LLJ is crucial to accurately simulating and properly timing the upscale growth of

an MCS, allowing more accurate MCS forecasts at later times. MCS QPF skill later in the evening was more dependent on the accuracy of the LLJ potential temperature and moisture forecasts, especially around 0600 UTC.

The present research raises additional questions. Why did MAEs for LLJ parameters in weakly forced regimes show little correlation with MCS QPF skill in convection-allowing forecasts and why did some WRF configurations behave very differently from the majority regarding the statistical significance for correlations between the accuracy of several simulated LLJ parameters and QPF skill? These questions require more extensive research into the role the individual microphysics and planetary boundary layer schemes play within numerical simulations of MCSs in both synoptic LLJ regimes. In addition, MUCAPE and MUCIN fields along with smaller-scale features such as gravity waves need more careful evaluation, especially in type A cases, where gravity wave induced forcing for ascent and buoyancy field characteristics may have the biggest impact on weakly forced MCSs in numerical forecasts. Finally, the differences in which parameters correlated well with QPF skill were often substantial between the two types of LLJ cases. Part II discusses the behavior of model LLJ and non-LLJ parameter errors as a function of LLJ type in more detail.

Acknowledgments. This research was sponsored by the National Science Foundation (NSF) under Grant AGS-1222383. Additional acknowledgment is provided to the NSF and National Centers for Environmental Prediction (NCEP) for allowing the author to partake in the NSF–NCEP visiting scientist program through an NSF supplement to AGS-1222383, where feedback from NOAA employees at the Storm Prediction Center, Environmental Modeling Center, and National Severe Storms Laboratory (NSSL) was received. Gratitude is extended to Dr. Adam Clark at NSSL for his guidance and code for calculating equitable threat scores using a neighborhood approach. Acknowledgement is also given to Dr. Tsing-Chang Chen and Dr. Raymond Arritt at Iowa State University's Department of Geologic and Atmospheric Sciences for their input regarding LLJ-type classification and to Dr. Mark Kaiser at Iowa State University's Department of Statistics for advice on determining the statistical significance for Spearman rank correlation values. Concepts for analyzing the geostrophic and ageostrophic wind fields in NCL were based on calculations provided by the University of Bergen's Geophysical Institute. Acknowledgment is given to Brandon J. Fisel of Iowa State University for suggesting the quantifying of the LLJ based on the 65th percentile, and to Daryl Herzmann, Dave Flory, Dr. Justin Glisan, Zachary Mangin, and Ben Moser for IT and programming support. The authors would also like to thank Dr. Russ S. Schumacher and the two anonymous reviewers of this manuscript for their insights and recommendations for improvements.

REFERENCES

Adams-Selin, R. D., S. C. Van Den Heever, and R. H. Johnson, 2013: Sensitivity of bow-echo simulation to microphysical parameterizations. *Wea. Forecasting*, **28**, 1188–1209, doi:10.1175/WAF-D-12-00108.1.

Ashley, W. S., T. L. Mote, P. G. Dixon, S. L. Trotter, E. J. Powell, J. D. Durkee, and A. J. Grundstein, 2003: Distribution of mesoscale convective complex rainfall in the United States. *Mon. Wea. Rev.*, **131**, 3003–3017, doi:10.1175/1520-0493(2003)131<3003:DOMCCR>2.0.CO;2.

Augustine, J. A., and F. Caracena, 1994: Lower-tropospheric precursors to nocturnal MCS development over the central United States. *Wea. Forecasting*, **9**, 116–135, doi:10.1175/1520-0434(1994)009<0116:LTPTNM>2.0.CO;2.

Blackadar, A. K., 1957: Boundary layer wind maxima and their significance for the growth of nocturnal inversions. *Bull. Amer. Meteor. Soc.*, **38**, 283–290.

Blanchard, D. O., 1990: Mesoscale convective patterns of the southern high plains. *Bull. Amer. Meteor. Soc.*, **71**, 994–1005, doi:10.1175/1520-0477(1990)071<0994:MCPOTS>2.0.CO;2.

Bonner, W. D., 1968: Climatology of the low level jet. *Mon. Wea. Rev.*, **96**, 833–850, doi:10.1175/1520-0493(1968)096<0833:COTLLJ>2.0.CO;2.

——, and J. Paegle, 1970: Diurnal variations in boundary layer winds over the south-central United States in summer. *Mon. Wea. Rev.*, **98**, 735–744, doi:10.1175/1520-0493(1970)098<0735:DVIBLW>2.3.CO;2.

Bryan, G. H., and H. Morrison, 2012: Sensitivity of a simulated squall line to horizontal resolution and parameterization of microphysics. *Mon. Wea. Rev.*, **140**, 202–225, doi:10.1175/MWR-D-11-00046.1.

Clark, A. J., W. A. Gallus Jr., and M. L. Weisman, 2010: Neighborhood-based verification of precipitation forecasts from convection-allowing NCAR WRF model simulations and the operational NAM. *Wea. Forecasting*, **25**, 1495–1509, doi:10.1175/2010WAF2222404.1.

Coniglio, M. C., J. Y. Hwang, and D. J. Stensrud, 2010: Environmental factors in the upscale growth and longevity of MCSs derived from the Rapid Update Cycle analyses. *Mon. Wea. Rev.*, **138**, 3514–3539, doi:10.1175/2010MWR3233.1.

——, J. Correia Jr., P. T. Marsh, and F. Kong, 2013: Verification of convection-allowing WRF model forecasts of the convective boundary layer using sounding observations. *Wea. Forecasting*, **28**, 842–862, doi:10.1175/WAF-D-12-00103.1.

Conover, W. J., 1971: *Practical Nonparametric Statistics*. 2nd ed. John Wiley and Sons, 493 pp.

Cotton, W. R., M.-S. Lin, R. L. McAnelly, and C. J. Tremback, 1989: A composite model of mesoscale convective complexes. *Mon. Wea. Rev.*, **117**, 765–783, doi:10.1175/1520-0493(1989)117<0765:ACMOMC>2.0.CO;2.

Duda, J. D., and W. A. Gallus Jr., 2013: The impact of large-scale forcing on skill of simulated convective initiation and upscale

evolution with convection-allowing grid spacings in the WRF. *Wea. Forecasting*, **28**, 994–1018, doi:10.1175/WAF-D-13-00005.1.

Ebert, E. E., 2008: Fuzzy verification of high-resolution gridded forecasts: A review and proposed framework. *Meteor. Appl.*, **15**, 51–64, doi:10.1002/met.25.

French, A. J., and M. D. Parker, 2010: The response of simulated nocturnal convective systems to a developing low-level jet. *J. Atmos. Sci.*, **67**, 3384–3408, doi:10.1175/2010JAS3329.1.

Fritsch, J. M., R. J. Kane, and C. R. Chelius, 1986: The contribution of mesoscale convective weather systems to the warm-season precipitation in the United States. *J. Climate Appl. Meteor.*, **25**, 1333–1345, doi:10.1175/1520-0450(1986)025<1333:TCOMCW>2.0.CO;2.

Hamill, T. M., 1999: Hypothesis tests for evaluating precipitation forecasts. *Wea. Forecasting*, **14**, 155–167, doi:10.1175/1520-0434(1999)014<0155:HTFENP>2.0.CO;2.

Hane, C. E., J. A. Haynes, D. L. Andra, and F. H. Carr, 2008: The evolution of morning convective systems over the U.S. Great Plains during the warm season. Part II: A climatology and the influence of environmental factors. *Mon. Wea. Rev.*, **136**, 929–944, doi:10.1175/2007MWR2016.1.

Helland, I. S., 1987: On the interpretation and use of R^2 in regression analysis. *Biometrics*, **43**, 61–69, doi:10.2307/2531949.

Higgins, R. W., Y. Yao, E. S. Yarosh, J. E. Janowiak, and K. C. Mo, 1997: Influence of the Great Plains low-level jet on summertime precipitation and moisture transport over the central United States. *J. Climate*, **10**, 481–507, doi:10.1175/1520-0442(1997)010<0481:IOTGPL>2.0.CO;2.

Hong, S.-Y., and J.-O. J. Lim, 2006: The WRF single-moment 6-class microphysics scheme (WSM6). *J. Korean Meteor. Soc.*, **42**, 129–151.

——, Y. Noh, and J. Dudhia, 2006: A new vertical diffusion package with an explicit treatment of entrainment processes. *Mon. Wea. Rev.*, **134**, 2318–2341, doi:10.1175/MWR3199.1.

Hu, X.-M., J. W. Nielsen-Gammon, and F. Zhang, 2010: Evaluation of three boundary layer schemes in the WRF model. *J. Appl. Meteor. Climatol.*, **49**, 1831–1843, doi:10.1175/2010JAMC2432.1.

Janjić, Z. I., 1994: The step-mountain eta coordinate model: Further developments of the convection, viscous sublayer, and turbulence closure schemes. *Mon. Wea. Rev.*, **122**, 927–945, doi:10.1175/1520-0493(1994)122<0927:TSMECM>2.0.CO;2.

Jankov, I., and W. A. Gallus Jr., 2004: MCS rainfall forecast accuracy as a function of large-scale forcing. *Wea. Forecasting*, **19**, 428–439, doi:10.1175/1520-0434(2004)019<0428:MRFAAA>2.0.CO;2.

Jirak, I. L., and W. R. Cotton, 2007: Observational analysis and predictability of mesoscale convective systems. *Wea. Forecasting*, **22**, 813–838, doi:10.1175/WAF1012.1.

——, ——, and R. L. McAnelly, 2003: Satellite and radar survey of mesoscale convective system development. *Mon. Wea. Rev.*, **131**, 2428–2449, doi:10.1175/1520-0493(2003)131<2428:SARSOM>2.0.CO;2.

Lin, Y., and K. E. Mitchell, 2005: The NCEP stage II/IV hourly precipitation analyses: Development and applications. Preprints, *19th Conf. on Hydrology*, San Diego, CA, Amer. Metoer. Soc., 1.2. [Available online at http://ams.confex.com/ams/Annual2005/techprogram/paper_83847.htm.]

Mapes, B. E., T. T. Warner, and M. Xu, 2003: Diurnal patterns of rainfall in northwestern South America. Part III: Diurnal gravity waves and nocturnal convection offshore. *Mon. Wea. Rev.*, **131**, 830–844, doi:10.1175/1520-0493(2003)131<0830:DPORIN>2.0.CO;2.

Markowski, P., and Y. Richardson, 2010: *Mesoscale Meteorology in Midlatitudes.* John Wiley and Sons, 407 pp.

Mason, I., 1989: Dependence of the critical success index on sample climate and threshold probability. *Aust. Meteor. Mag.*, **37**, 75–81.

Mellor, G. L., and T. Yamada, 1982: Development of a turbulence closure model for geophysical fluid problems. *Rev. Geophys. Space Phys.*, **20**, 851–875, doi:10.1029/RG020i004p00851.

Mesinger, F., 2008: Bias adjusted precipitation threat scores. *Adv. Geosci.*, **16**, 137–142, doi:10.5194/adgeo-16-137-2008.

Mitchell, M. J., R. W. Arritt, and K. Labas, 1995: A climatology of the warm season Great Plains low-level jet using wind profiler observations. *Wea. Forecasting*, **10**, 576–591, doi:10.1175/1520-0434(1995)010<0576:ACOTWS>2.0.CO;2.

Myers, J. L., and A. D. Well, 2003: *Research Design and Statistical Analysis*. 2nd ed. Chapman and Hall, 760 pp.

Nakanishi, M., 2001: Improvement of the Mellor–Yamada turbulence closure model based on large-eddy simulation data. *Bound.-Layer Meteor.*, **99**, 349–378, doi:10.1023/A:1018915827400.

NCAR/UCAR/EOL, 2015: GCIP/EOP surface: Precipitation NCEP/EMC 4-km gridded data (GRIB) stage IV data. Subset used: May 2007–June 2014, accessed 13 July 2015. [Available online at http://data.eol.ucar.edu/cgi-bin/codiac/fgr_form/id=21.093.]

NCDC, 2015a: NCEP numerical weather prediction models North American Meso-Scale Grid 218. Subset used: May 2007–June 2014, accessed 23 February 2015. [Available online at http://nomads.ncdc.noaa.gov/cgi-bin/ncdc-ui/definecollection.pl?model_sys=nam&model_name=nam&grid_name=218.]

——, 2015b: NCEP Rapid Update Cycle (13 km RUC). Subset used: May 2007–June 2014, accessed 23 February 2015. [Available online at nomads.ncdc.noaa.gov/data/ruc13/.]

Pan, Z., M. Segal, and R. W. Arritt, 2004: Role of topography in forcing low-level jets in the central United States during the 1993 flood-altered terrain simulations. *Mon. Wea. Rev.*, **132**, 396–403, doi:10.1175/1520-0493(2004)132<0396:ROTIFL>2.0.CO;2.

Parish, T. R., and L. D. Oolman, 2010: On the role of sloping terrain in the forcing of the Great Plains low-level jet. *J. Atmos. Sci.*, **67**, 2690–2699, doi:10.1175/2010JAS3368.1.

Peters, J. M., and P. J. Roebber, 2014: Synoptic control of heavy-rain-producing convective training episodes. *Mon. Wea. Rev.*, **142**, 2464–2482, doi:10.1175/MWR-D-13-00263.1.

Roberts, N. M., and H. W. Lean, 2008: Scale-selective verification of rainfall accumulations from high-resolution forecasts of convective events. *Mon. Wea. Rev.*, **136**, 78–97, doi:10.1175/2007MWR2123.1.

Schumacher, R. S., 2009: Mechanisms for quasi-stationary behavior in simulated heavy-rain-producing convective systems. *J. Atmos. Sci.*, **66**, 1543–1568, doi:10.1175/2008JAS2856.1.

——, and R. H. Johnson, 2009: Quasi-stationary, extreme-rain-producing convective systems associated with midlevel cyclonic circulations. *Wea. Forecasting*, **24**, 555–574, doi:10.1175/2008WAF2222173.1.

——, A. J. Clark, M. Xue, and F. Kong, 2013: Factors influencing the development and maintenance of nocturnal heavy-rain-producing convective systems in a storm scale ensemble. *Mon. Wea. Rev.*, **141**, 2778–2801, doi:10.1175/MWR-D-12-00239.1.

Skamarock, W. C., and Coauthors, 2008: A description of the Advanced Research WRF version 3. NCAR Tech. Note NCAR/TN-475+STR, 113 pp., doi:10.5065/D68S4MVH.

Snively, D. V., and W. A. Gallus Jr., 2014: Prediction of convective morphology in near-cloud-permitting WRF model

simulations. *Wea. Forecasting*, **29**, 130–149, doi:10.1175/WAF-D-13-00047.1.

Song, J., K. Liao, R. L. Coulter, and B. M. Lesht, 2005: Climatology of the low-level jet at the southern Great Plains atmospheric boundary layer experiments site. *J. Appl. Meteor.*, **44**, 1593–1606, doi:10.1175/JAM2294.1.

Stensrud, D. J., 1996: Importance of low-level jets to climate: A review. *J. Climate*, **9**, 1698–1711, doi:10.1175/1520-0442(1996)009<1698:IOLLJT>2.0.CO;2.

Thompson, G., P. R. Field, W. D. Hall, and R. M. Rasmussen, 2008: Explicit forecasts of winter precipitation using an improved bulk microphysics scheme. Part II: Implementation of a new snow parameterization. *Mon. Wea. Rev.*, **136**, 5095–5115, doi:10.1175/2008MWR2387.1.

Thompson, R. L., R. Edwards, J. A. Hart, K. L. Elmore, and P. M. Markowski, 2003: Close proximity sounding within supercell environments obtained from the Rapid Update Cycle. *Wea. Forecasting*, **18**, 1243–1261, doi:10.1175/1520-0434(2003)018<1243:CPSWSE>2.0.CO;2.

Uccellini, L. W., 1980: On the role of upper tropospheric jet streaks and leeside cyclogenesis in the development of low-level jets in the Great Plains. *Mon. Wea. Rev.*, **108**, 1689–1696, doi:10.1175/1520-0493(1980)108<1689:OTROUT>2.0.CO;2.

——, and D. R. Johnson, 1979: The coupling of upper and lower tropospheric jet streaks and implications for the development of severe convective storms. *Mon. Wea. Rev.*, **107**, 682–703, doi:10.1175/1520-0493(1979)107<0682:TCOUAL>2.0.CO;2.

Weisman, M. L., C. Davis, W. Wang, K. W. Manning, and J. B. Klemp, 2008: Experiences with the 0–36-h explicit convective forecasts with the WRF-ARW model. *Wea. Forecasting*, **23**, 407–437, doi:10.1175/2007WAF2007005.1.

Wexler, H., 1961: A boundary layer interpretation of the low-level jet. *Tellus*, **13**, 368–378, doi:10.1111/j.2153-3490.1961.tb00098.x.

Whiteman, C., X. Bian, and S. Zhong, 1997: Low-level jet climatology from enhanced rawinsonde observations at a site in the southern Great Plains. *J. Appl. Meteor.*, **36**, 1363–1376, doi:10.1175/1520-0450(1997)036<1363:LLJCFE>2.0.CO;2.